Perovskite Colloidal Nanocrystal Solar Cells: Current Advances, Challenges, and Future Perspectives

Wenqiang Yang, Seung-Hyeon Jo, and Tae-Woo Lee*

The power conversion efficiencies (PCEs) of polycrystalline perovskite (PVK) solar cells (SCs) (PC-PeSCs) have rapidly increased. However, PC-PeSCs are intrinsically unstable without encapsulation, and their efficiency drops during large-scale production; these problems hinder the commercial viability of PeSCs. Stability can be increased by using colloidal PVK nanocrystals (c-PeNCs), which have high surface strains, low defect density, and exceptional crystal quality. The use of c-PeNCs separates the crystallization process from the film formation process, which is preponderant in large-scale fabrication. Consequently, the use of c-PeNCs has substantial potential to overcome challenges encountered when fabricating PC-PeSCs. Research on colloidal nanocrystal-based PVK SCs (NC-PeSCs) has increased their PCEs to a level greater than those of other quantum-dot SCs, but has not reached the PCEs of PC-PeSCs; this inferiority significantly impedes widespread application of NC-PeSCs. This review first introduces the distinctive properties of c-PeNCs, then the strategies that have been used to achieve high-efficiency NC-PeSCs. Then it discusses in detail the persisting challenges in this domain. Specifically, the major challenges and solutions for NC-PeSCs related to low short-circuit current density J_{sc} are covered. Last, the article presents a perspective on future research directions and potential applications in the realm of NC-PeSCs.

1. Introduction

In recent years, solar cell (SC) technologies have been remarkably improved, particularly by the development of perovskite (PVK) SCs. Metal-halide PVKs have the general chemical structure ABX$_3$, where A is a monovalent cation, either organic methylammonium (MA$^+$) or formamidine (FA$^+$), or inorganic (Cs$^+$); B is a divalent metal cation like Pb^{2+} or Sn^{2+}; and X is a halide anion (Cl$^-$, Br$^-$, or I$^-$). The crystal structure consists of corner-shared [BX$_6$]$^{4-}$ octahedra.[1,2] The compositional adjustability of PVKs permits tuning of their bandgap E_g across the spectrum from violet to near-infrared by the use of diverse cations and anions.[3,4] In addition, the distinctive crystal structure of PVK engenders exceptional optoelectronic properties, including a high absorption coefficient, long carrier diffusion length, and high defect tolerance. Attributed to these superior optoelectronic properties, PVKs have substantial potential in photovoltaics. Remarkably, the power conversion efficiencies (PCEs) of single-junction polycrystalline PVK SCs (PC-PeSCs) have increased from 3.6% to a record-high 26.1%, which rivals those of single-junction silicon SCs.[5] However the commercial utilization of PC-PeSCs is impeded by their deficiencies, notably inadequate long-term operational stability, and PCEs drop during scale-up fabrication.[6] The inherent soft crystal structure of PVKs renders them exceedingly susceptible to ambient conditions. Exposure to water, oxygen, heat, or light can trigger their decomposition into lead halide and volatile alkylammonium iodide, and this transition degrades their structural integrity and decreases their PCEs.[7,8] Furthermore, polycrystalline PVK films have nonuniform crystallization, which results in a PCE drop in large-area devices.[9,10] Consequently, to advance their commercial viability, their stability and uniformity of crystallization must be increased. colloidal PVK nanocrystals (c-PeNCs), including colloidal

W. Yang
Institute of Atomic Manufacturing
International Research Institute for Multidisciplinary Science
Beihang University
Beijing 100191, China
W. Yang, S.-H. Jo, T.-W. Lee
Department of Materials Science and Engineering
Seoul National University
1 Gwanak-ro, Gwanak-gu, Seoul 08826, Republic of Korea
E-mail: twlees@snu.ac.kr

T.-W. Lee
Research Institute of Advanced Materials
Seoul National University
1 Gwanak-ro, Gwanak-gu, Seoul 08826, Republic of Korea
T.-W. Lee
Interdisciplinary program in Bioengineering
Institute of Engineering Research
Seoul National University
1 Gwanak-ro, Gwanak-gu, Seoul 08826, Republic of Korea
T.-W. Lee
Soft Foundry
Seoul National University
1 Gwanak-ro, Gwanak-gu, Seoul 08826, Republic of Korea

quantum dots, and nanocrystals of sizes slightly above exciton Bohr diameters, have good structural stability and superior crystallinity, so they may present solutions to these problems.[11–14]

c-PeNCs undergo size-induced high lattice strain and as a result, have exceptional phase stability and low defect densities within their crystals.[15] Their nanoscale size induces charge confinement effects, which yield narrow emission widths, high photoluminescence quantum yield (PLQY), and some unique carrier behaviors.[16,17] Moreover, the use of c-PeNC films can separate the film formation process from the crystallization process, thus they can be competitive in large-area devices.[18] Because of these advantages, c-PeNCs have widespread utility in optoelectronic devices, including SCs, light-emitting diodes (LEDs), artificial neuromorphic devices, and scintillators.[19–24] And, owing to its high PLQY, c-PeNCs can also serve as a down-conversion layer to transform UV light to visible light, thus reducing the photon energy loss and improving the stability in PeSCs.[25,26] Besides, due to the similar crystal structure of c-PeNCs to polycrystalline PVK, c-PeNCs have been employed to boost up the PCEs of PC-PeSCs, by mitigating the defects of PVK films and/or building a graded heterojunction.[27–29]

The prevalent method to produce c-PeNC involves colloidal synthesis, wherein AX reacts with BX_2 in the presence of long-chain organic ligands such as oleic acid (OA), oleylamine (OAm), or octylamine.[30] $MAPbBr_3$ NCs of 6-nm size were first synthesized in 2014.[31] Subsequently, ligand-assisted re-precipitation (LARP) method for synthesizing colloidal $MAPbX_3$ NCs was developed.

LARP entails dissolving the PVK precursor in N-dimethylformamide, and subsequently dropping the solution into a solution of long-chain ligands in toluene.[32] The solubility difference among precursors drives formation of c-PeNCs. Moreover, LARP method also can be used to in-situ form the protection layer for c-PeNCs, resulting good stability and high PLQY of c-PeNCs.[33] LARP is a popular method to synthesize c-PeNCs, in which $X = Br^-$, but high-quality c-PeNCs in which $X = I^-$ are difficult to obtain because they are degraded by the polar solvents that are used in LARP.[32]

Hot injection is an alternative method that enables production of c-PeNCs of various compositions and sizes ranging from 5 to 20 nm.[34,35] Hot injection is a traditional method to synthesize cadmium chalcogenide NCs,[36] and now is also the most efficient method to obtain c-PeNCs with a uniform size distribution, especially for c-PeNCs in which $X = I^-$.

The maturation of synthesis technology has stimulated progress in c-PeNC optoelectronic devices. The concept of c-PeNC SCs (NC-PeSCs) was reported in 2014 and the initial NC-PeSCs paper in 2016 used $CsPbI_3$ NCs and achieved a remarkable PCE = 10.77%.[23,24,37] Since then, intensive investigation and improvement strategies such as in situ doping, ligand exchanges, and post-treatments have markedly increased the PCE of NC-PeSCs.[38,39] Currently, the highest certified PCE for NC-PeSCs is 19.1%, which surpasses all other SCs that use colloidal NCs.[5] This achievement emphasizes the considerable potential of c-PeNCs in advancing the landscape of photovoltaic technologies.

However, the PCE of NC-PeSCs is still inferior to the PCEs of PC-PeSCs. Several factors contribute to this deficit. The inherent cha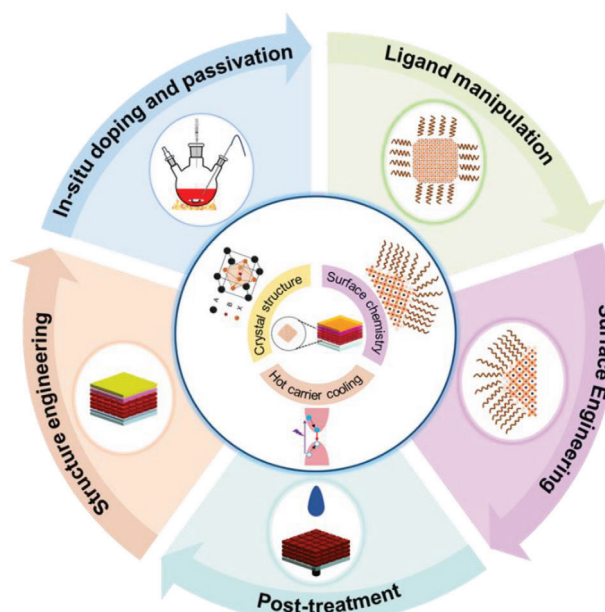rge confinement that occurs as a result of the small nanoparticle size elevates the exciton binding energy (E_b), and thereby impairs the efficient exciton dissociation that is crucial for generating free carriers.[40,41] This impairment increases the number of excitons that engage in radiative recombination, and thus diminishes the pool of carriers that are available for conversion to photocurrent.

The insulating nature of organic long-chain ligands within c-PeNCs significantly hampers carrier transport across c-PeNC films.[42] To solve this problem, researchers have endeavored to replace long-chain ligands with short-chain ligands. However, the complete removal of long-chain ligands remains challenging, so some insulating components remain. Moreover, purification and ligand exchange processes to remove long-chain ligands often yield a c-PeNC film surface that bears numerous dangling bonds, which act as non-radiative recombination sites.[38] Consequently, challenges related to difficult exciton dissociation, inefficient carrier transport, and surface defects notably limit the PCE of NC-PeSCs, and particularly contribute to a lower short-circuit current density (J_{sc}) than in PC-PeSCs.

However, recent progress in increasing the PCE of NC-PeSCs and addressing outstanding challenges remains limited. Therefore, this review presents first the intrinsic properties of c-PeNCs, then the current effective methods to increase PCEs (**Figure 1**). We also summarize unresolved challenges and present future perspectives in the domain of NC-PeSCs.

Figure 1. Structure of this review, including the fundamental properties of c-PeNCs, and approaches to make high-efficiency NC-PeSCs.

2. Intrinsic Properties of Colloidal PVK Nanocrystals

2.1. Crystal Structure

The crystal structure of c-PeNCs (**Figure 2a**), is composed of a network involving corner-shared $[BX_6]^{4-}$ octahedra and a selectively-inserted A cation, which fills the rigid octahedral hole that is
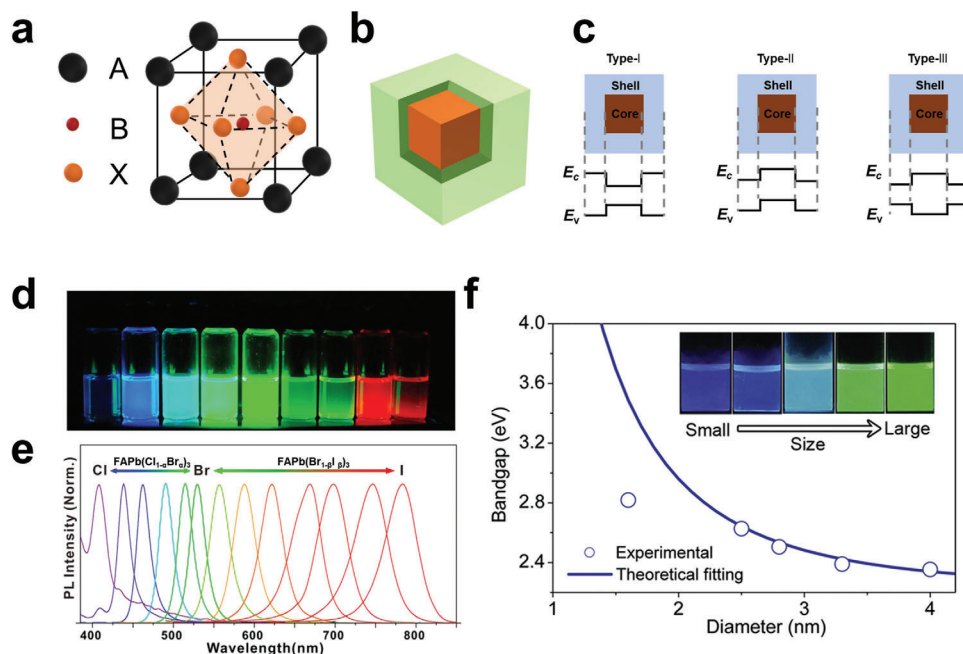
**ADVANCED
SCIENCE NEWS**

www.advancedsciencenews.com

**ADVANCED
MATERIALS**

www.advmat.de

Figure 2. a) Schematic of PVK crystal structure. b) Schematic of core–shell c-PeNCs. c) Energy-band diagram of type-I and type-II c-PeNCs. d,e) FAPbX$_3$ NCs dispersed in toluene under UV irradiation ($\lambda_{peak} = 365$ nm) and corresponding PL emission spectra. Reprinted with permission.[43] Copyright 2017, American Chemical Society. f) Comparison between the experimental and theoretical fitting results of different-sized MAPbBr$_3$ NCs in the diameter range of 1.6–3.9 nm; inset: digital photograph of different-sized MAPbBr$_3$ NCs dispersed in toluene under the illumination of 365 nm. Reprinted with permission.[44] Copyright 2016, Elsevier.

formed by the 12 nearest X atoms.[45] Diverse combinations of A, B, and C ions facilitate tunable PVK compositions, which can be exploited to modulate optoelectronic properties. However, to achieve the desired PVK phase, each component must be selected to have an appropriate ionic radius. This goodness of compositional combination is quantified using the Goldschmidt tolerance factor $t = (R_A + R_X)/(\sqrt{2}(R_B + R_X))$, where R_A, R_B, and R_X represent the ionic radii of the corresponding ions.[46,47] When $0.8 < t < 1.0$, the PVK assumes a black phase at room temperature; this phase is favorable for SC applications. When $t \approx 0.8$, the formed PVK is unstable. When $t < 0.8$, the compound typically assumes an orthorhombic or tetragonal structure at room temperature. Conversely, $t > 1$ leads to the formation of low-dimensional structures due to the oversized A or B cations.[48,49]

Under ambient conditions, CsPbI$_3$ has $t \approx 0.8$, so it predominantly assumes an orthorhombic phase.[50] Obtaining cubic CsPbI$_3$ requires elevated temperature, high pressure, or additional external stress.[50–52] However, cubic CsPbI$_3$ NCs can be obtained in ambient conditions, as a result of high surface energy and size-induced lattice strain, and therefore present better phase stability than polycrystalline CsPbI$_3$ films.[53] But CsPbI$_3$ NCs also have inherently-soft ionic bonding, which makes them susceptible to degradation upon exposure to polar solvents or environmental stressors (e.g., light, heat, oxygen).[54,55]

Application of a shell over the c-PeNC cores is increasingly used to increase stability and optoelectronic properties (Figure 2b).[56] An adeptly-designed shell shields against solvent and environmental damage, and also offers benefits such as amenability to energy-band manipulation, accelerated exciton

separation, increased PLQY, and suppression of non-radiative recombination and blinking.[57–59] To create a flawless shell, two criteria must be met: appropriate band alignments and minimal lattice mismatch.

To manipulate carrier behavior, the band alignment between the core and shell stands must be appropriate.[60] Photoelectron spectroscopy and density functional theory are usually used to predict the energy-band alignment condition between the core and shell.[61] Three predominant band alignment conditions for core–shell NCs are the type I, II, and III configurations (Figure 2c), and have distinct influences on carrier behavior. In type I, the shell has a wider bandgap than the core, so the conduction band and valence band of cores are located inside the band gap of shells; as a result, the holes or electrons are confined inside the core and difficult to separate to form free carriers. This attribute reduces photovoltaic efficiency but is beneficial for luminance applications.[56] Usually, a c-PeNC without a shell is type I, because the long-chain ligands on the surface of c-PeNC are insulating. In type II, the energy band alignment between cores and shells is staggered, so only the electron or hole is partially confined in the core. This structure is beneficial for exciton dissociation.[62] In type III, the core has a wider bandgap than the shell, which is just the reverse of type I.

The second criterion is minimal lattice mismatch, generally < 15%.[63,64] Excessive lattice mismatch induces lattice distortion and generates defect states between the core and shell, which lead to NC degradation.[65] Shell overcoating (e.g., Cs$_4$PbBr$_6$, CdS, PbSe, SiO$_2$) on c-PeNC cores has been realized to tune the properties of c-PeNCs.[47,66–68] Moreover, the use of multi-shell

2401788 (3 of 25)

**ADVANCED
SCIENCE NEWS**

www.advancedsciencenews.com

**ADVANCED
MATERIALS**

www.advmat.de

structures (e.g., SiO_2/PVDF, SiO_2/Al_2O_3,) can concurrently increase their optoelectronic properties and stability.[69,70]

The bandgap of c-PeNCs can be readily tuned by many methods. Owing to the ionic structure of c-PeNCs, altering the c-PeNC composition readily tunes their bandgap in the range from blue to red (Figure 2d,e).[43] Furthermore, decrease in crystal size toward the Bohr radius yields quantum confinement effects which lead to discrete energy levels.[71] Consequently, controlling the size of c-PeNCs also enables tuning of the energy band structure,[72] with c-PeNC bandgap increasing as particle size is decreased (Figure 2f).[44]

Theoretical analyses indicate that PVKs have high defect tolerance, with most defects localized in the shallow regions of conduction and valence bands, with minimal interstitial and anti-site defects due to their high formation energy.[73,74] As a result, c-PeNCs have tunable bandgaps, narrow emission spectra, and high PLQYs.[75] Given these advantages, c-PeNCs are increasingly recognized as highly promising materials for use in both SCs and LEDs.[18,76]

2.2. Surface Properties

As material sizes are reduced to the nanoscale, the surface-to-volume ratio amplifies, so the significance of surface properties increases. Despite the introduction of long-chain ligands during synthesis to stabilize c-PeNCs, the weak dynamic bonding between c-PeNC surfaces and these ligands renders them susceptible to loss during synthesis and purification processes, so numerous under-coordinated defects can form on the surface.[78,79] Moreover, when the A-site comprises organic cations (MA^+ or FA^+), these organic cations are susceptible to polar solvents and are therefore prone to be washed away along with the long-chain ligands.[80,81] Consequently, the abundant under-coordinated atoms and vacancy sites provide as non-radiative recombination pathways, and thereby degrade the optoelectronic properties of c-PeNCs. Therefore, the development of effective methods to increase the PCE of NC-PeSCs requires understanding of these surface properties.

We present $CsPbBr_3$ NCs as the example to understand the surface properties of c-PeNCs. By cutting one out of an orthorhombic distorted idealized cubic bulk lattice, the upper bound for the anion/lead ratio is derived, and it allows proposing three types of termination, considering the upper and lower bounds to their anion/lead (Br/Pb) stoichiometry (**Figure 3a**).[77] The outermost layer of c-PeNC formed by Cs and Br atoms gives a terminal structure of $[CsPbBr_3](PbBr_2)<CsBr>$. When Cs is partially replaced by long-chain ligands (A), the c-PeNC surface presents a terminal structure of $[CsPbBr_3](PbBr_2)<ABr>$. Both of $[CsPbX_3](PbBr_2)<CsBr>$ and $[CsPbX_3](PbBr_2)<ABr>$ structures have a $CsPbX_3$ core and a $PbBr_2$ inner shell. The $[CsPbBr_3](PbBr_2)<CsBr>$ structure has no dangling bonds, but in $[CsPbBr_3](PbBr_2)<ABr>$, if the long-chain ligands fail to entirely cover the vacancy of Cs atoms due to steric hindrance and dynamic equilibrium between the c-PeNC surface and solution, some dangling bonds may occur; they provide non-radiative recombination centers, which degrade the optoelectronic properties. When the outmost layer has X/Pb ratio < 3, the c-PeNC surface can present a termination structure

$[CsPbBr_3](ABr)<PbBr_2>$. However, this termination type is unlikely due to unfavorable formation energy and necessitates much dense ligand coverage. Thus, the surface termination of c-PeNC usually requires A-site cation or ligands to avoid the formation of dangling bonds. Furthermore, c-PeNCs are typically synthesized in a lead-rich environment, which inevitably results in under-coordinated lead species or halide vacancies.[82] Hence, AX salts are commonly used to treat as-synthesized c-PeNCs, with the goal of reducing surface defects.[83]

Long-chain ligands are indispensable in the preparation of c-PeNC. Extensive research has demonstrated their functions in modulating nucleation, growth, stability, and defects.[84–86] Considering the covalent bond classification, ligands on c-PeNC surfaces can be categorized into three types: Z, X, and L (Figure 3b).[87] Z-type ligands, such as K^+ and Na^+ act as electron acceptors, accepting a lone electron pair from halide anions, and are regarded as Lewis acids.[88,89] X-type ligands, such as alkylammonium salts, alkyl acids, and zwitterionic molecules function as one-electron donors to surface cations or anions.[90,91] L-type ligands, such as alkylamine and alkyl-phosphine oxide, serve as two-electron donors, and typically coordinate with Pb^{2+}.[92]

Generally, pairs of alkyl-carboxylic acids and alkyl-amines (e.g., OA and OAm) are used as initial ligands to synthesize c-PeNC. Alkyl-carboxylic acids chelate with lead atoms on c-PeNC surfaces, whereas alkyl-amines bind to halide atoms by $[X\cdots H-N^+]$ hydrogen bonding.[94,95] Although these two types of bonds are very weak, they have important functions in the formation of c-PeNCs. The quantities of these two ligands regulate the nucleation process of c-PeNCs. Insufficient OAm induces anisotropic growth, because long-chain ligands bind preferentially to crystal facets that have low packing density.[96] Conversely, excess OAm disperses the precursor, and thereby hinders formation of c-PeNCs.[97,98] The lengths of these two ligands also affect the size and shape of c-PeNCs, and inhibit them from forming large grains like polycrystalline films (**Figure 4**).[79,93] Short-chain amines only result in nanoplates, whereas long-chain amines could facilitate formation of NCs under high-temperature reactions. In addition, the length of acid primarily affects c-PeNC size rather than shape, but does affect NC or nanoplate size.

2.3. Hot-Carrier Cooling

When a semiconductor absorbs a photon that has energy approximately equal to or larger than its bandgap, an electron-hole pair is generated within the semiconductor material. If the photon energy exceeds the bandgap of an absorber, the excited carriers hold excess kinetic energy compared to the ground state carriers, and are termed as hot carriers. These hot carriers rapidly dissipate excess the energy as phonons within femtoseconds; this is the primary energy loss pathway in SCs.[103] Thus, exploiting hot carriers presents a way to achieve ultra-high PCE beyond the Shockley-Queisser limitation.[104]

Typically, hot carriers cool by three processes (**Figure 5a**).[105,106] 1) Electron-phonon coupling occurs within 1 ps. 2) Optical phonons convert to acoustic phonons; when carrier density is high, a hot-phonon bottleneck effect where the relaxation rate of phonons is reduced, will occur in this process. 3) Carriers emit acoustic phonons until the carriers reach thermal
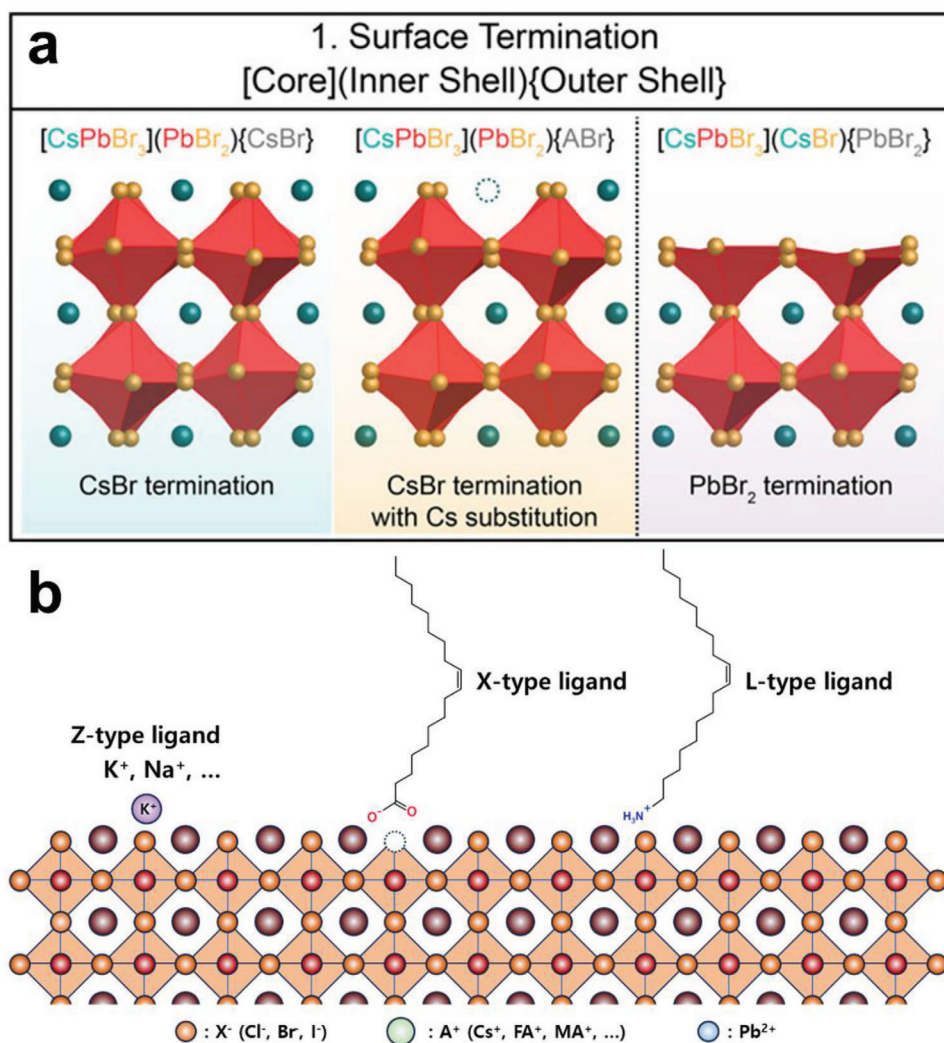
**ADVANCED
SCIENCE NEWS**

www.advancedsciencenews.com

**ADVANCED
MATERIALS**

www.advmat.de

Figure 3. a) Idealized surface termination of as-synthesized orthorhombic $CsPbBr_3$ NCs. Blue spheres: Cs atoms; yellow spheres: Br atoms. Pb atoms are located at the center of the red octahedra formed by Br. A corresponding to the outmost ligands. Reproduced with permission.[77] Copyright 2020, American Chemical Society. b) Representative Z-, X-, and L-type ligands.

equilibrium, and the hot carrier cools to lattice temperature. However, enhanced acoustic-optical phonon up-conversion may reheat carriers, so steps (2) and (3) can be repeated. After this process, if carrier intensity is high, non-radiative Auger heating may re-excite cooled carriers to high energy levels.[107]

Many studies have used transient spectroscopy to investigate the slow hot carrier cooling in c-PeNCs.[108–111] The cooling lifetime of hot carriers in c-PeNCs is affected by their components and size. Different components of c-PeNCs cool at different rates (Figure 5b). For instance, $CsPbI_3$ NCs cooling more slowly than $FAPbI_3$ NCs.[99] However, alloying Cs into $FAPbI_3$ NCs cannot efficiently decelerate the cooling rate of $FAPbI_3$ NCs. The fast cooling of $FAPbI_3$ NCs is ascribed to strong electron-phonon coupling that originates from the dynamic motion of the organic cations.[112]

The size of the c-PeNC also affects the cooling rate of hot carriers (Figure 5c).[100] As c-PeNC size decreases below the Bohr diameter, the energy levels become discrete with enlarged energy

spacing, so the cooling of hot carriers requires the emission of multiple phonons; this phonon bottleneck slows hot-carrier cooling significantly.[113,114]

The cooling rate of hot carriers is also affected by the external environment, including temperature and excitation intensity.[107,115] For example, hot-carrier cooling of c-PeNC can be modulated by the excitation intensity (Figure 5d).[101] Under low excitation intensity, hot-carrier cooling is typically slowed by the phonon bottleneck effect, but under high excitation intensity, especially at illumination greater than 1 sun, Auger heating significantly retards hot-carrier cooling by promoting acoustic-optical phonon up-conversion.[116] This effect is more evident in organic–inorganic cation alloyed c-PeNCs, due to the introduction of co-vibrational optical phonon modes by alloying organic cations and inorganic cations.[99]

Despite the slow hot-carrier cooling in c-PeNCs, extracting these hot carriers remains challenging. Hot-carrier extraction has been achieved in heterojunction of $MAPbBr_3$ NCs/Bphen due to

**ADVANCED
SCIENCE NEWS**

www.advancedsciencenews.com
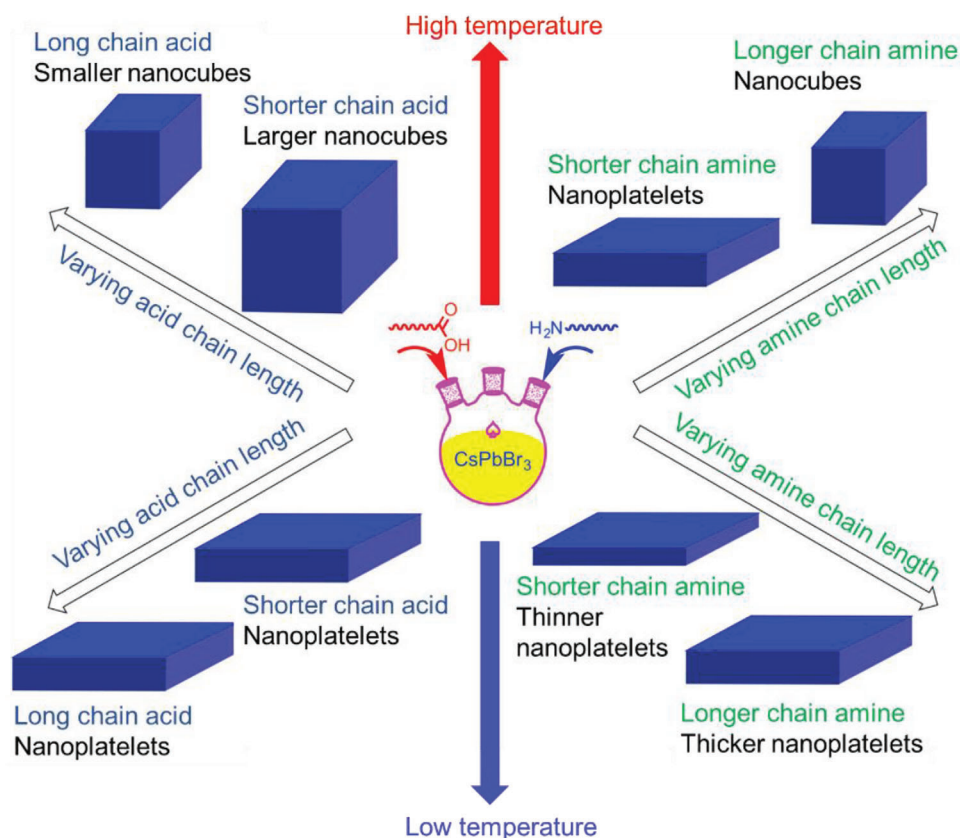
**ADVANCED
MATERIALS**

www.advmat.de

Figure 4. Dependence of shape and size on temperature and chain length of carboxylic acids and amines. Reproduced with permission.[93] Copyright 2016, American Chemical Society.

the high electron mobility and high lowest unoccupied molecular orbital (LUMO) of Bphen.[101] However, the high LUMO of Bphen conversely restricts the extraction of cold carriers, and thereby degrades SC PCE. Furthermore, contact with commonly-used electron-transporting layers like TiO$_2$ results in complete hot-carrier cooling before extraction (Figure 5e).[102] Thus, much progress is required before utilization of hot carriers by c-PeNCs is feasible. Utilizing hot carriers from c-PeNCs requires suitable charge acceptors with appropriate energy bands and high carrier mobility. Moreover, the carrier transport properties of c-PeNC film must be increased.

3. The Way to High-Efficiency PVK Colloidal Nanocrystal SCs

Since the first reported NC-PeSCs in 2016, their PCE has increased from 10.77% to 19.1%, as certified by the National Renewable Energy Laboratory (NREL).[5,37] Diverse strategies have been developed to achieve this increase. Here, we summarize five general strategies to achieve high-efficiency NC-PeSCs.

3.1. In-Situ Doping and Passivation

c-PeNCs are commonly synthesized using the hot injection method, particularly c-PeNCs that are intended for use in SCs.

This method involves injecting A-oleate precursor into a lead-halide precursor that has long-chain ligands, at temperatures ranging from 80 to 180 °C. Immediately after the solution has been cooled down to room temperature, it is purified using methyl acetate (MeOAc) as an anti-solvent to eliminate unreacted precursors and excess ligands. The synthesis process significantly influences c-PeNC quality, and subsequently affects the c-PeNC film quality. The tunable composition of c-PeNCs allows modulation of their physical and chemical properties by doping or ion exchange during synthesis. Thus, in-situ doping and passivation during synthesis have been used to achieve c-PeNCs that have uniform size distribution, low defect density, and good stability (**Figure 6a**).

Uniform size distribution of c-PeNCs is important to achieve compact and stable c-PeNC films. To achieve this uniformity, researchers have developed many strategies to optimize the synthesis process. 2D spacers like PEA$^+$, which are usually adopted in 2D polycrystalline PVKs, have also been introduced into c-PeNCs.[120] However, this kind of 2D spacer usually works as a short-chain ligand, and will not insert into the lattice as A-site cations. A ternary-precursor approach for c-PeNC synthesis uses different I-sources, such as ionic-type amine iodide salt PEAI, covalent-type iodide compound trimethylsilyl iodide (TMSI), and 2-iodo-2-methylpropane (TBI).[117] The choice of I-source influences uniformity and surface condition. For example, PEA can partly replace the long-chain ligands, but at the cost of
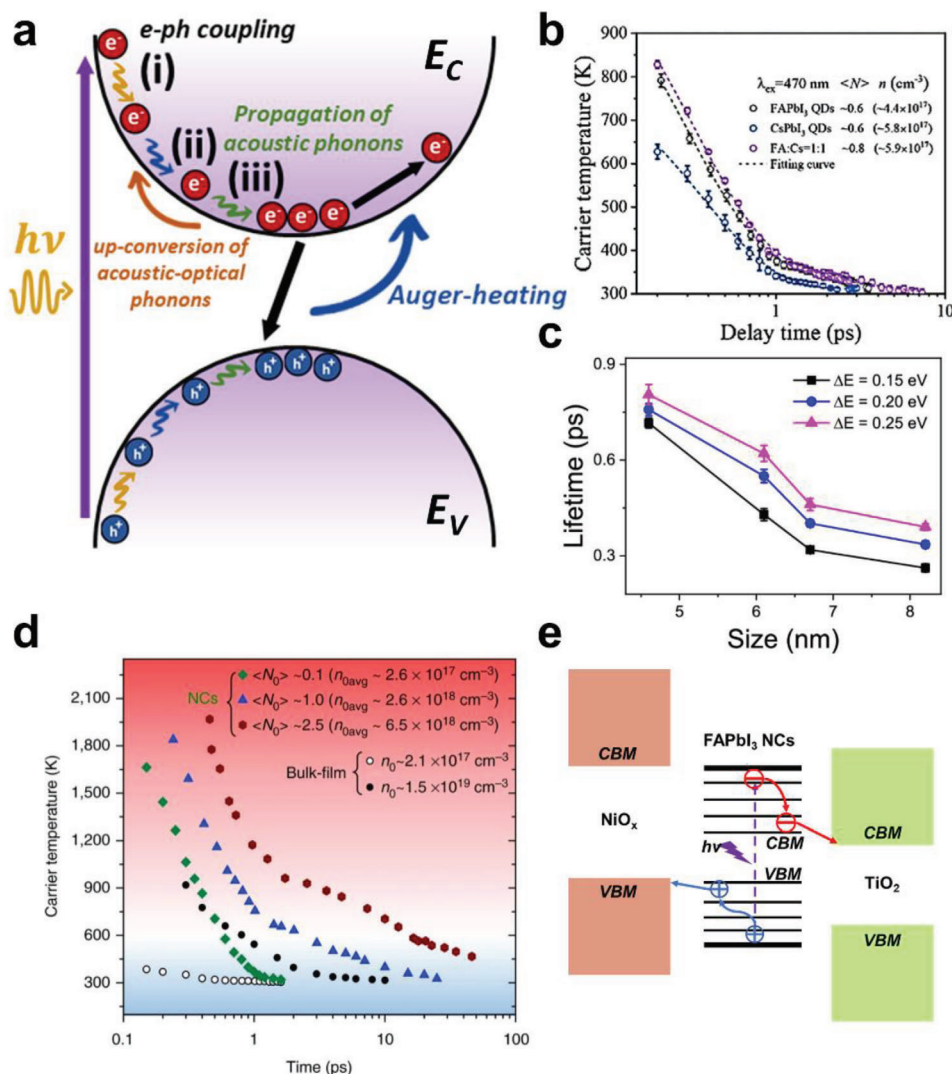
**ADVANCED
SCIENCE NEWS**

www.advancedsciencenews.com

**ADVANCED
MATERIALS**

www.advmat.de

Figure 5. a) Schematic diagram of hot-electron relaxation process. b) Time-dependent carrier temperature for $FAPbI_3$, $CsPbI_3$, $FA_{0.5}Cs_{0.5}PbI_3$ NCs with an excitation light of 470 nm. Reproduced with permission.[99] Copyright 2023, Wiley-VCH. c) Size-dependent lifetime parameters for hot-carrier dynamics. Reprinted with permission.[100] Copyright 2021, American Chemical Society. d) Hot-carrier temperature as a function of delay time for medium $MAPbBr_3$ NCs and bulk films with different carrier densities. Reprinted with permission.[101] Copyright 2017, Springer Nature. e) Schematic of hot and cold carrier relaxation and transfer at the $FAPbI_3$ NCs/TiO_2 and $FAPbI_3$ NCs/NiO_x interfaces. Reproduced with permission.[102] Copyright 2020, Elsevier.

reducing the uniformity of c-PeNCs. In contrast, TMSI yields c-PeNCs that have uniform size distribution and cubic morphology (Figure 6b). Subsequent use of nucleophilic trioctylphosphine (TOP) to neutralize the by-products and unreacted TMSI on the c-PeNC surface, yielded highly-orientated c-PeNC films with a reduced number of defects, and a PCE of 16.25%.[117]

The A-site species also affects the characteristics of c-PeNCs. $CsPbI_3$ NCs have increased thermal stability, but they have phase instability owing to their small tolerance factor. In contrast, $FAPbI_3$ has a suitable tolerance factor with a smaller band gap and better charge transporting than $CsPbI_3$, due to the expanded lattice structure and enhanced spin-orbit coupling in $FAPbI_3$.[121] Consequently, research efforts, whether focused on polycrystalline PVK films or c-PeNCs, often combine Cs with FA. However, for mixed-cation c-PeNCs, uniform size distribution is not sufficient to yield desirable optoelectronic properties, uni-

form elemental distribution is also necessary. Non-uniform elemental distribution causes both phase segregation and instability issues.[122]

Cross-exchange of cations in an OA-rich environment can be used to prepare homogeneous $Cs_{1-x}FA_xPbI_3$ NCs.[123] The presence of OA facilitated mild cation exchange, which yielded uniform size and uniform elemental distribution. More importantly, the synergistic effect of FA and ligands suppressed phase segregations and the formation of deep-energy-level defects induced by the insufficient coverage on the surface of c-PeNCs. The incorporation of FA also broadened the absorption spectra, and thereby increased light-harvesting ability and increased J_{sc}. NC-PeSCs that used these $Cs_{1-x}FA_xPbI_3$ NCs achieved a record PCE of 16.6%.

Homogeneous $FA_xCs_{1-x}PbI_3$ NCs with tunable stoichiometry and surface ligand chemistry have been synthesized using
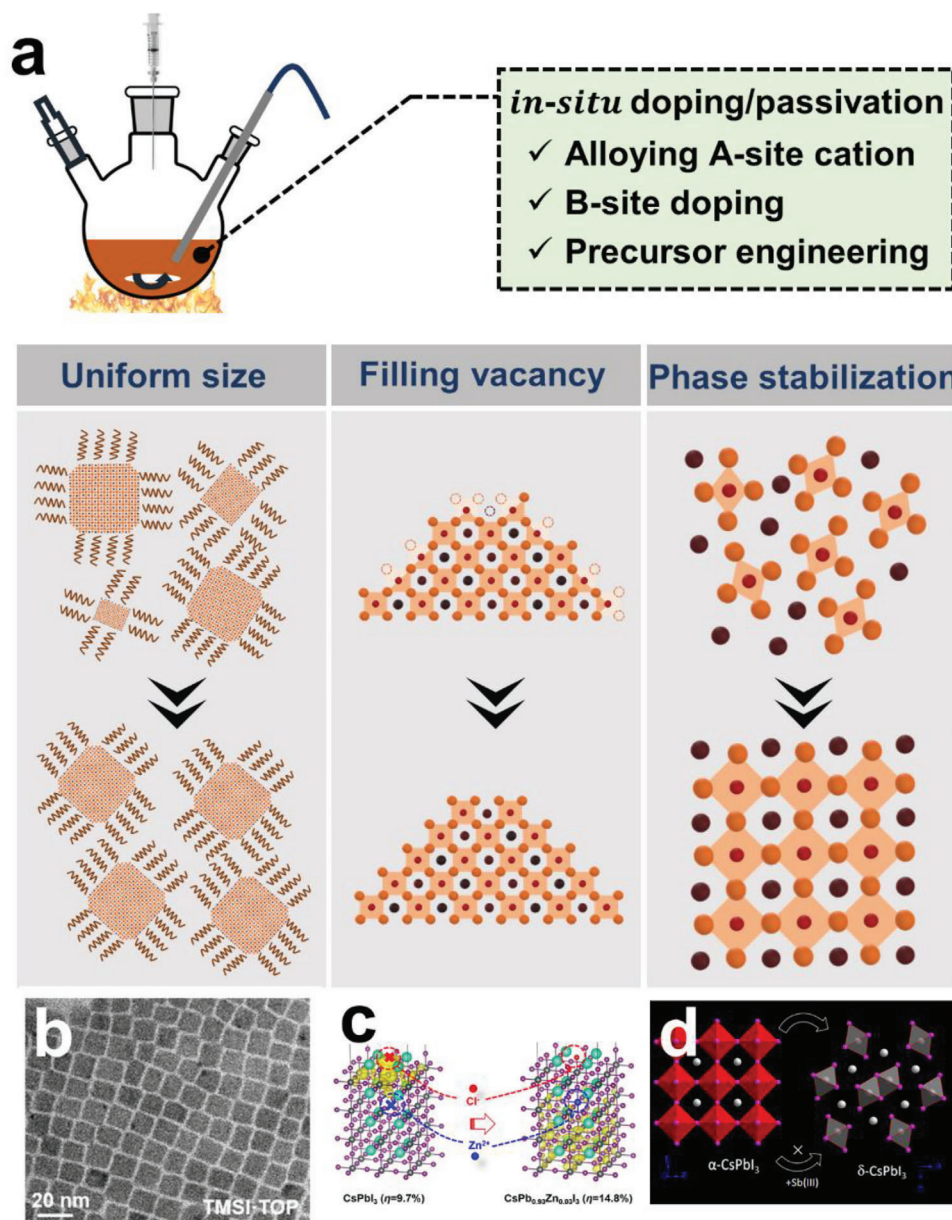
Figure 6. a) Schematic illustration of in-situ doping and passivation. b) TEM image of c-PeNCs that use ternary precursor. Reprinted with permission.[117] Copyright 2022, Wiley-VCH. c) Density state of $CsPbI_3$ NCs passivated by $ZnCl_2$. Reprinted with permission.[118] Copyright 2020, American Chemical Society. d) Illustration of Sb(III) stabilizing $CsPbI_3$ NCs. Reprinted with permission.[119] Copyright 2019, American Chemical Society.

an antisolvent-assisted in situ cation exchange method.[124] This method may provide the ability to obtain uniform size and elemental distribution, flattened energy landscape, and highly-oriented c-PeNC films, and contribute to the continuous increase in the charge transport of NC-PeSCs. As a result of these characteristics, the PCE was increased to 17.29%.

The B-site cation affects the stability of PVK crystals by altering the shape of the octahedra. However, the B-site has higher formation energy than the A-site and X-site, so exchange at the B-site presents greater challenges than changes at the other sites.[125] Small amounts of metal cations that are smaller than Pb, like Mn^{2+} and Zn^{2+}, can be alloyed into c-PeNCs to increase the tol-

erance factors and reduce the lattice constant, thereby increasing the phase stability. In situ doping of these metal cations can also reduce the defect density in as-synthesized c-PeNCs. For example, when $CsPb_{1-x}Zn_xI_3$ NCs were synthesized by hot injection with the addition of $ZnCl_2$, the $ZnCl_2$ could compensate for vacancy defects in c-PeNCs (Figure 6c).[118] The guest Zn^{2+} improved the local ordering of the PVK crystal and reduced the octahedral distortions. Besides, ZnI_2 can decrease the number of iodide vacancies, increase the stability of $CsPbI_3$ NC-PeSCs, and increase their PCE from 13.98% to 16.07%.[126] Zn doping increased the thermodynamic stability by increasing the formation energy and tolerance factor, whereas the additional halide ions
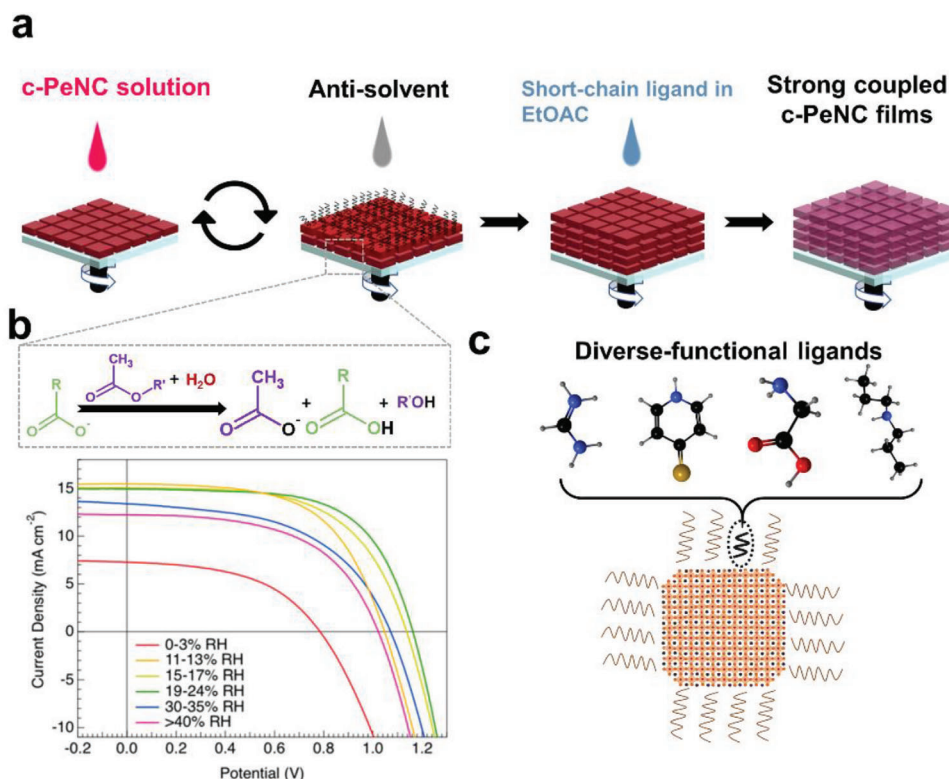
ADVANCED
SCIENCE NEWS

www.advancedsciencenews.com

ADVANCED
MATERIALS

www.advmat.de

Figure 7. a) Schematic of the c-PeNC film-deposition process in which anti-solvent is used to partially remove long-chain ligands, and a short-chain ligand in ethyl acetate is used to replace the residual long-chain ligands. b) Top: schematic of the process of removing oleic acid during deposition of c-PeNC film, and bottom: current density–voltage curves of CsPbI$_3$ NC-PeSCs fabricated at six humidity levels ranging from 3 to 40% RH. Reproduced with permission.[95] Copyright 2018, American Chemical Society. c) Schematic of diverse functional ligands used to replace the original long-chain ligands.

in the reaction system could regulate the growth and decrease the number of vacancy defects in c-PeNCs, thereby increasing PLQY.

Rare-earth elements have also been introduced into PVK materials and have shown a positive effect on PC-PeSCs. Heterovalent antimony (Sb(III)) ions can also be introduced into the B-site of cubic CsPbI$_3$ NCs during synthesis.[119] Replacement of a limited amount of Pb with Sb(III) in the lattice increases the phase stability and optical stability in ambient air (Figure 6d). In situ ytterbium (Yb) doping by adding ytterbium acetate to the lead precursor during synthesis of CsPbI$_3$ NCs allows some Yb^{3+} ions to occupy the Pb^{2+} site, and stabilizes the crystal lattice by improving the tolerance factor.[127] Doping with Yb can also decrease the number of Cs$^+$ and I$^+$ vacancies, and thereby decrease the number of surface defects and lattice vacancies; consequently, the PCEs and device stability under ambient conditions were increased.[127]

In addition to element dopings, high mobility semiconductor materials have also been doped into c-PeNC films to enhance its conductivity. For instance, μ-graphene (μGR) was used to crosslink CsPbI$_3$ NCs, thereby establishing a charge transport channel between c-PeNCs to enhance carrier transport within c-PeNC films.[128] Moreover, the introduction of μGR has been demonstrated to suppress the agglomeration triggered by thermal and moisture, improving the stability of NC-PeSCs.[128]

In conclusion, in-situ doping, passivation, and ion exchange during synthesis represent effective methods to improve c-PeNC quality, and thereby increase the PCE of NC-PeSCs.

3.2. Ligand Manipulation

Long-chained insulating ligands facilitate the growth and dispersion of c-PeNCs during synthesis. Typically, one terminal of the ligand binds dynamically to the c-PeNC surface, and the other forms an alkyl dangling chain.[129] The commonly-used ligands are OA and OAm, which are insulating. During the layer-by-layer process assembling of c-PeNCs, large amounts of these insulating long-chain ligands are left in the c-PeNC film, where they obstruct carrier transport, and thereby degrade the PCE of NC-PeSCs. To obtain c-PeNC films that have high carrier mobility and strong electronic coupling between c-PeNCs, the long-chain ligands must be replaced using liquid-state or solid-state ligand exchange. Varied ligands, differing in chain lengths and functional groups, have been used to replace these insulating ligands.

A two-step solid-state ligand-exchange method is widely used.[87,115] It involves immersing c-PeNC films in an anti-solvent of MeOAc to remove OA, where hydrolysis of MeOAc generates methanol and acetic acid, which then protonates oleate ligands to yield acetate and free oleic acid (**Figure 7a,b**). Then after film deposition, they were treated with FAI as short ligand in ethyl

ADVANCED
SCIENCE NEWS

www.advancedsciencenews.com

**ADVANCED
MATERIALS**

www.advmat.de

acetate (EtOAc) to replace OAm (Figure 7a). This method yields c-PeNC films with decent electronic-coupling for NC-PeSCs. Notably, the ligand-exchange efficiency in this method is significantly affected by environmental humidity (atmospheric water), not by the water in MeOAc.[95] The hydrolysis reaction requires the attachment of atmospheric water vapor to oleate ligands on the c-PeNC surface. As a result, the device PCE was correlated with the environmental humidity (Figure 7b).[95] Also, the duration of FAI treatment is crucial, because prolonged exposure degrades c-PeNC films and causes FA insertion into the c-PeNC crystal, whereas short durations are ineffective in ligand exchange. Thus, this method should be conducted very carefully. Subsequently, various functional and different length short-ligands have been developed to increase the PCE of NC-PeSCs (Figure 7c).

Hydrophilic trait of FA induces humidity instability, and has therefore prompted efforts to prevent FA insertion into $CsPbI_3$ crystals during ligand exchange.[130] Glycine is a hydrophobic ligand that can be used as a dual-passivation ligand in a facile one-step ligand strategy.[131] Theoretical analysis revealed that the glycine could simultaneously fill both the A-site vacancies and the iodine vacancies on the surface of c-PeNCs at the same time, and can thereby decease defect densities and enhance charge transports. Also, the hydrophobic properties of glycine increased the humidity stability of $CsPbI_3$ NC-PeSCs, and increased their PCE from 11.69% to 13.66% with good stability.

The functional groups in ligands are important to ligand exchange efficiency. Thus, tuning functional groups in ligands is an efficient method to obtain high mobility c-PeNC films. P-mercaptopyridine (4-MP) was introduced as short ligands by immersing $CsPbI_3$ NC films in EtOAc containing 4-MP ligands, that can increase the electronic coupling in the films and increase their structure stability.[132] The N atom and -SH moiety in 4-MP strengthen the linking ability between ligands with the core of $CsPbI_3$ NCs, and thereby efficiently passivate the surface defects of c-PeNCs. The 4-MP linker reduces distances between Pb atoms on (100) facets, thereby increasing electronic coupling in c-PeNC films and consequently significantly improving PCEs and stability of NC-PeSCs under ambient conditions for over 2 months.

Facilitating the acylation reaction between the amino group in short ligands and the carboxyl group in OA is an effective way to remove long ligands. The chemical alkalinity of organic amine ligands significantly influences the reactivity of this acylation process.[133] With the same alkyl chain length, secondary amine has higher alkalinity than tertiary amine, primary amine, and amino. Tertiary amine lacks hydrogen atoms, so it cannot directly react with OA. Besides, the type, number, and length of chains around the amino group affect the reactivity.[133] Alkyl chains are electron-donating groups, so they can increase the density of the electron cloud, and thereby increase the reactivity. In contrast, phenyl groups are electron-withdrawing, and decrease the density of the electron cloud, thereby reducing the reactivity. Consequently, a secondary amine with double alkyl chains is more reactive than other organic amine ligands, presents an accelerated acylation reaction, and facilitates ligand-exchange efficiency.

Additionally, conductive ligands that can delocalize the wave function from c-PeNC films have been used as short ligands to increase the charge-separation efficiency in c-PeNCs films. A facile strategy can build a hetero-interface by introducing a conjugated small molecule, 2,2′-[[6,6,12,12-tetrakis(4-hexylphenyl)−6,12-dihydrodithieno[2,3-d:2′,3′-d′]-s-indaceno[1,2-b:5,6-b′]dithiophene-2,8-diyl]bis[methylidyne(3-oxo-1H-indene-2,1(3H)-diylidene)]]bis[propanedinitrile]   (ITIC) in EtOAc, to replace the long-chained ligands.[134] The ITIC remains on the surface of c-PeNCs and thereby forms a heterojunction-like structure, which facilitates charge transfer from the c-PeNC to ITIC, and thus increases the exciton separation efficiency and the carrier-collection efficiency. This strategy has boosted the PCEs of $FAPbI_3$ NC-PeSCs to 12.7%. Except this, triphenyl phosphite (TPPI) is a bulky conductive ligand, which can help to balance carrier transport, improve charge transport, and decrease carrier recombination.[135] This method has been used to develop the first electroluminescent SCs that use c-PeNCs.

In summary, deliberate surface ligand engineering holds promise for increasing NC-PeSC PCE and stability. The goal is to use short ligands to remove long-chain ligands to improve inter-coupling of c-PeNC films while maintaining their integrity and stability. Achievement of these goals will require comprehensive understanding and careful design of replacement ligands.

3.3. Surface Engineering

c-PeNCs have high surface-to-volume ratio, so the surface has a strong influence on the quality of c-PeNCs. The washing and re-precipitation processes cause ligand losses, which result in an abundance of under-coordinated sites on c-PeNC surfaces.[139] Additionally, during ligand exchange using polar solvents like MeOAc or EtOAc, the loss of A-site cations and iodine causes defect centers on c-PeNC surfaces.[140] These defects capture carriers and decrease the carrier density that is available to be converted to photocurrent. They also induce non-radiative recombination loss and accelerated ion migration, which degrade device PCE. Thus, surface engineering by adjusting capping-ligands, passivating defects, and reconstructing surface structures can increase the efficiency of NC-PeSCs (**Figure 8**a).

Increasing the strength of dynamic bonds between ligands and c-PeNC surface can suppress formation of surface defects. This strength depends on the length of ligands and the functional groups on it. A mixture of OA/OAm (C18) and octanoic acid/octylamine (C8) which is shorter than C18 can be used as a capping layer to synthesize $CsPbI_3$ NCs.[134] Compared to C18, C8 has stronger adsorption energy with c-PeNCs (Figure 8b), and therefore suppresses formation of surface defects.

Replacing long-chain ligands with short ones can also passivate the surface defects on c-PeNC films. Short conductive aromatic ligands benzylamine (BZA) and benzoic acid (BA), have been used as capping ligands to synthesize $MAPbBr_3$ NCs. These ligands effectively passivate c-PeNC surfaces and significantly increase both PLQY and carrier lifetime.[141]

Loss of ligands during purification can distort the lattice of c-PeNCs, thereby loosening the stacking and reducing the stability of c-PeNC films. To address this problem, aprotic TMSI that has an inverted triangular-pyramidal cationic structure can be used as a ligand to rivet the c-PeNC surface.[142] This method can fill the surface vacancies and exploit the steric effect to impart tensile strains from the c-PeNC surface into the bulk, thus improving
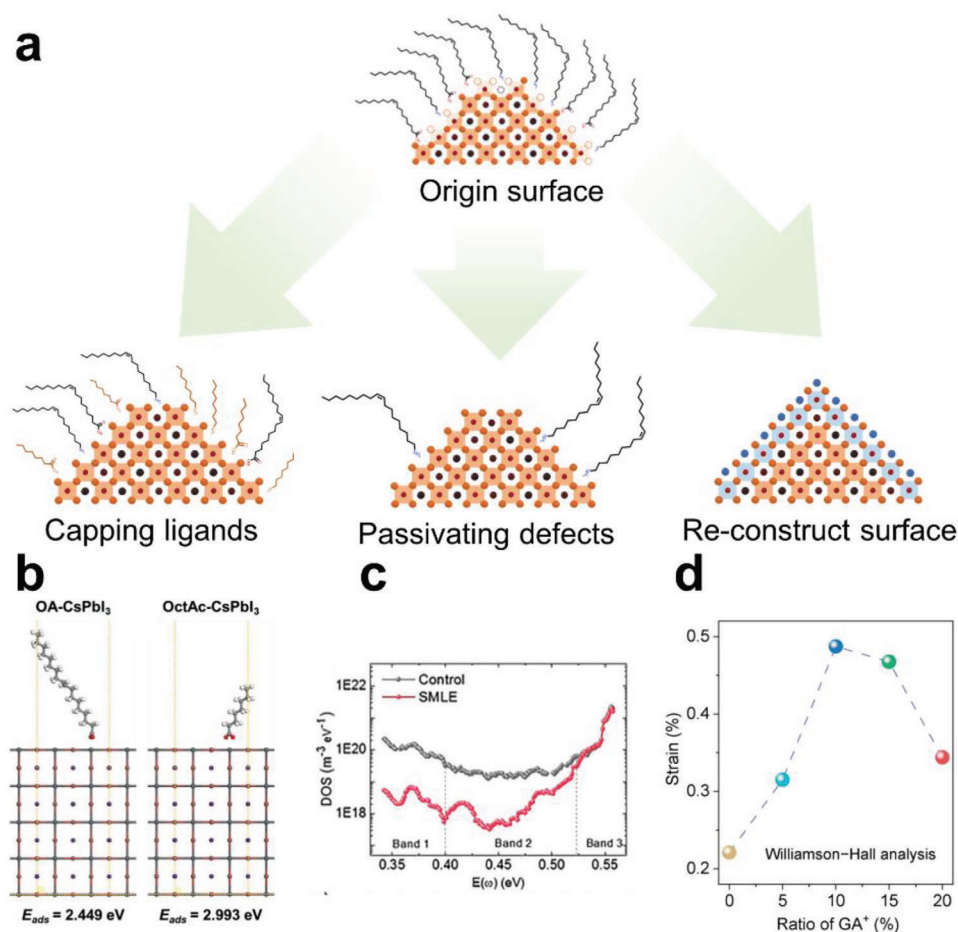
**ADVANCED
SCIENCE NEWS**

www.advancedsciencenews.com

**ADVANCED
MATERIALS**

www.advmat.de

Figure 8. a) Schematic of diverse surface-engineering approaches. b) Theoretical adsorption energy of various ligands with CsPbI$_3$ NCs. Reproduced with permission.[136] Copyright 2019, Wiley-VCH. c) Trap density of states (DOS) for control and MAI-passivated devices. Reprinted with permission.[137] Copyright 2023, Wiley-VCH. d) Strain values extracted by Williamson–Hall analysis for CsPbI$_3$ and GA-CsPbI$_3$ NCs with different GA ratios. Reprinted with permission.[138] Copyright 2022, American Chemical Society.

the structural regularity, optoelectronic properties, and stability of c-PeNCs.

Defects on the surface of c-PeNCs are mostly a result of the absence of monovalent cations. To counter this problem, the incorporation of monovalent cations effectively passivates defects in polycrystalline PVK films into c-PeNCs. For example, phenylethyl ammonium (PEA$^+$)/2-(4-fluorophenyl) and ethyl ammonium (FPEA$^+$) passivated the surface defects of CsPbI$_3$ NCs and yielded PCE = 14.65% with excellent stability.[143] The prolonged device stability is due to the hydrophobicity of PEA$^+$ and FPEA$^+$, which protects the c-PeNC film from moisture.

A-site vacancies are usually generated together with X-site vacancies. Monovalent cations cannot passivate both of these types. L-phenylalanine (L-PHE) is a bi-functional ligand. It has been used as a passivation agent for CsPbI$_3$ NCs.[144] L-PHE has stronger bonding with c-PeNCs than the native ligands with c-PeNCs, so it can coordinate with both cations and ions on the c-PeNC surface. Thus, it effectively reduces the defect density, increases the vacancy-formation energy, and therefore increases PCE and stability in NC-PeSCs. The use of an ionic liquid, 1-propyl-3-methylimidazolium iodide ([Pmim]I) can modulate the

surface of CsPbI$_3$ NCs.[145] [Pmim]I has high polarity and electron donating ability, so the lone pair electrons on the nitrogen of imidazole ring within [Pmim]I can fill dangling orbitals on the surface of CsPbI$_3$ c-PeNCs, and thereby decrease the Cs and I vacancies at the same time. In addition, when the optimal amount of methylammonium iodide (MAI) is dissolved in anti-solvent to treat the FAPbI$_3$ NC solution, the MAI concurrently passivates the A- and X-site vacancies.[137] As a result, the defect density was significantly reduced (Figure 8c).

Methods to engineer the surface structure of c-PeNCs have been developed. Surface matrix curing (SMC) is a strategy to restore the surface of c-PeNCs by exploiting the unimolecular nucleophilic substitution reaction between tert-butyl iodide (TBI) and nucleophile trioctylphosphine (TOP);[146] the use of this reaction to introduce sufficient iodide ions to fill the iodide vacancies on the surface matrix of CsPbI$_3$ NCs greatly improved their optoelectronic properties, decreased the non-radiative recombination loss induced by iodide vacancies, and therefore yielded a high PCE = 16.21%. Similarly, a method to in situ grow an atomic guanidinium lead iodide PVK matrix on CsPbI$_3$ NCs induces substantial surface strain and efficient coupling in the
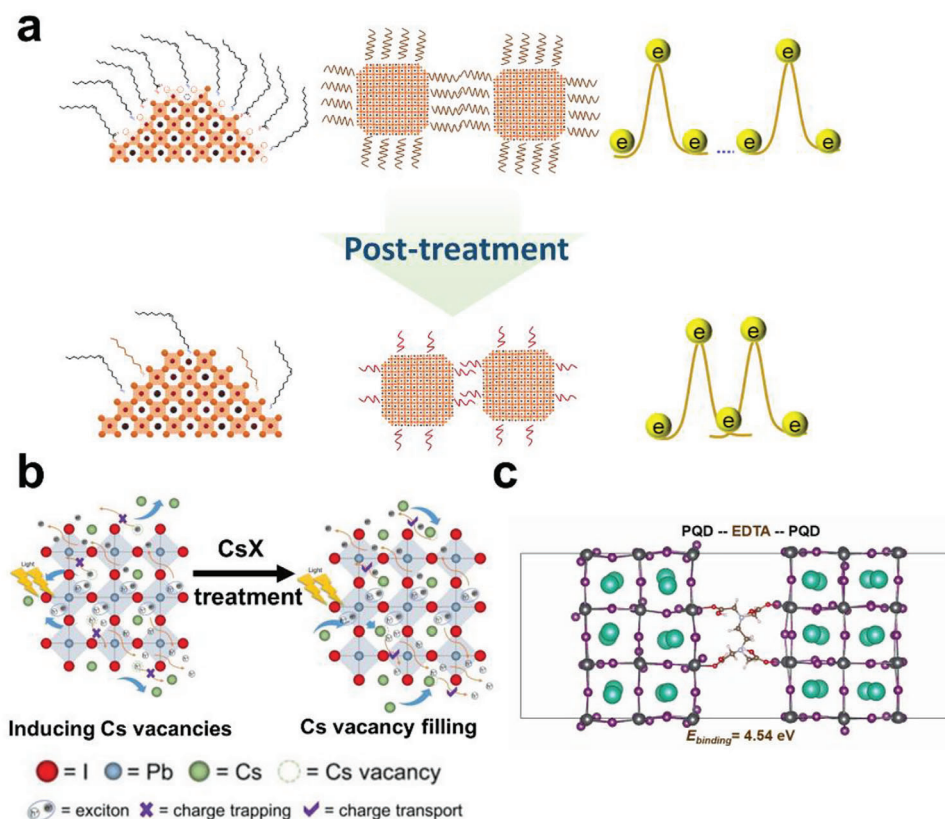
Figure 9. a) Schematic illustration of post-treatment effect on c-PeNC surface, film, and electronic-coupling condition. b) Schematic illustration of CsPbI$_3$ NC film post-treated by CsX. Reproduced with permission.[149] Copyright 2019, Wiley-VCH. c) Calculated structure of the charge density of EDTA bridging adjacent c-PeNCs. Reprinted with permission.[150] Copyright 2022, Elsevier.

c-PeNC films to improve the stability and optoelectronic properties of NC-PeSCs (Figure 8d).[138]

The nanoscale nature of the grains of c-PeNCs permits modulation of the interface between c-PeNCs. A hybrid interfacial heterojunction composed of CsPbI$_3$ NC/phenyl-C61-butyric acid methyl ester (PCBM)[146] can bond with the under-coordinated Pb^{2+} ions on the c-PeNC surface through carboxyl groups of PCBM, and build an exciton cascade between the CsPbI$_3$ NC films and electron transporting layers (ETL), which decrease surface defects and promoted exciton dissociation. In addition, the introduction of PCBM increased adhesion between c-PeNC films and ETLs. This method achieved PCE = 15.1% for rigid NC-PeSCs, and PCE = 12.3% for flexible NC-PeSCs.

The surface of FAPbI$_3$ c-PeNCs can be easily reconfigured using formamidine thiocyanate (FASCN). It is an ionic liquid and can increase the electronic coupling of FAPbI$_3$ c-PeNC films.[147] FASCN is sufficiently soluble in MeOAC, so fine control of the concentration can effectively manage the surface ligand density. FA$^+$ and SCN$^-$ pseudo-halide anions can facilitate the removal of pristine long-chain ligands and concurrently passivate the targeted surface defects. Consequently, the FAPbI$_3$ NC-PeSC had a high PCE = 14.47% and improved stability, which are attributed to reduced trap-assisted recombination and increased electronic coupling. Similarly, the surface of FAPbI$_3$ c-PeNCs could also reconstructed by immersing it in MASCN solution.[148] Different from reconfigured by FASCN, reconstructing FAPbI$_3$ c-PeNCs

film by MASCN would result in a 6.20 nm MAPbI$_3$ capping layer, leading to better energy alignment with the hole transporting layer (HTL) and enhanced device stability.

The development of effective methods to engineer the surfaces of c-PeNCs has great potential to decrease the number of trap states on c-PeNC surfaces, and to obtain excellent PCE of NC-PeSCs.

3.4. Post-Treatment

The low ligand-exchange efficiency results in residual long-chain ligands in c-PeNCs films, and additional defects would be introduced during ligand exchange process. Consequently, numerous studies have focused on post-treating c-PeNC films to further increase the electronic-coupling within c-PeNC films and decrease defect density (**Figure 9a**).

Post-treating polycrystalline PVK films with AX salts has been widely applied in PC-PeSCs, and effectively increases the device PCE. Cs$^+$ has an appropriate radius and good conductivity, so it is increasingly used as an effective passivation agent for CsPbI$_3$ NCs. Comparison of cesium salts, such as cesium acetate (CsAc), cesium iodide (CsI), cesium carbonate (Cs$_2$CO$_3$), and cesium nitrate (CsNO$_3$), established that CsAc was the most effective post-treatment agent to passivate to CsPbI$_3$ NCs (Figure 9b).[149] Passivation using CsAc notably increased the mobility, lifetime, and

**ADVANCED
SCIENCE NEWS**

www.advancedsciencenews.com

**ADVANCED
MATERIALS**

www.advmat.de

diffusion length of free carriers in the c-PeNC film, and thereby elevated its J_{sc} and fill factor. This method stabilized the structure, and as a result, increased stability against moisture.

CsAc also could passivate the interfaces between c-PeNC films and transporting layers. Modification of the surface of mesoscopic-TiO$_2$ by using a solution of CsAc in MeOAc facilitates penetration of c-PeNC into m-TiO$_2$, and as a result, increases the efficiency of carrier extraction from c-PeNC films.[151] The surface of m-TiO$_2$ bears numerous Cs$^+$ ions, which passivate the surface of CsPbI$_3$ NCs, and increase the charge coupling between the ETLs and CsPbI$_3$ NC films.

Besides, post-treatment of c-PeNC film by using sodium acetate in MeOAc effectively removes long-chain ligands and minimizes the number of surface trap states.[152] Thus, alkali metal salts can be effective passivation agents to decrease the number of surface defects and increase the carrier transport in NC-PeSCs.

Some monovalent organic cations have also been used to post-treat c-PeNC films. Layer-by-layer FAI treatment has been used to fabricate inverted CsPbI$_3$ NC-PeSCs, which had PCE = 13.1%.[153] In this process, FA replaced long-chain ligands and cured film voids that originated due to volume loss during assembly of c-PeNC film. Alloying Cs with FA yielded suitable tolerance factors to improve the phase stability of CsPbI$_3$ NC films. Thus, this method provided a way to fabricate inverted NC-PeSCs; such a method has rarely been reported. Besides, ligand exchange by using MAI in IPA to post-treat the FAPbI$_3$ NC films was also demonstrated effectively in replacing the long-chain oley ligands and suppressing the formation of δ phase, resulting in a record PCE of 18.1%.[154]

Salts of guanidinium (GA) and phenylalkylammonium (PEA) can decrease the number of defects, and therefore have also been used to post-treat polycrystalline PVK film and c-PeNC film.[1,155] The use of a guanidinium thiocyanate (GASCN) solution in EtOAc to post-treat the c-PeNC films, followed by mild annealing, drove GA$^+$ to replace remaining long-chain ligands and induce surface-matrix formation on the CsPbI$_3$ NC surface. As a result, charge mobility and carrier diffusion length were increased, so PCE = 15.21% was obtained. This method was also effective for CsPbBr$_3$ NCs, and therefore may be applicable in semitransparent photovoltaics.[86]

However, the use of FA and GA cations can decrease the humidity stability of c-PeNC films. To solve this problem, hydrophobic phenethylammonium (PEA) cations can be used to post-treat the c-PeNC films.[120] The PEA efficiently anchored to the surface of c-PeNCs, where it replaces long-chain ligands while increasing the stability and electronic coupling of c-PeNC films. The method increased the V_{oc} to 1.23 V, and achieved good stability. These monovalent organic cations usually occupied the A-site in the PVK crystal, and thus effectively decreased the numbers of A-site vacancies and under-coordinated lead species. These monovalent organic cations are also short, so they can partially replace long-chain ligands, and thereby increase the electronic coupling within c-PeNC films.

Layer-by-layer deposition of c-PeNC films entails anti-solvent rinsing after deposition of each layer, so the surface environment becomes chaotic. As a result, single-functional molecules are ineffective in passivating all defect states. Multi-dentate molecules can improve the optoelectronic characteristics and stability of PC-PeSCs. Therefore, these molecules have been eval-

uated for c-PeNC film post-treatment.[156] Post-treating c-PeNC films with multi-dentate ligands like ethylene diamine tetraacetic acid (EDTA) also improved the optoelectronic properties of NC-PeSCs.[150] EDTA could effectively passivate the surface defects of c-PeNCs by peeling under-coordinated Pb^{2+} ions from the c-PeNC surface and filling I$^-$ vacancies in it. Moreover, EDTA removes long-chain ligands and provides a charge bridge that crosslinks adjacent c-PeNCs (Figure 9c), and thereby strengthens the electronic coupling of c-PeNC films.[150] These CsPbI$_3$ NC-PeSCs achieved PCE = 15.25%.

The solvent used to post-treat c-PeNC film should be carefully selected. The use of solvents with appropriate dielectric constant and acidity can efficiently remove long-chain ligands without introducing defects. Solvents that have low dielectric constants and weak acidity cannot effectively remove long-chain ligands, but solvents with high dielectric constant and strong acidity can degrade c-PeNCs.[158] Systematic screening of several solvents identified 2-pentanol (2-PeOH) as the post-treatment agent that yielded the highest PCE.[158]

The nanometer size of crystallites in c-PeNC films induces charge confinement, which impedes exciton dissociation and decreases the number of carriers that can be converted to photocurrent. These effects constrain the PCE, so it remains much lower in NC-PeSCs than in PC-PeSCs. This constraint can be overcome by increasing the size of the crystallites.

A simple re-assembling process (RP) for c-PeNC films, with the use of a blend of pyridine and 2-isopropanol (IPA) to post-treat c-PeNC films (**Figure 10**a) can simultaneously increase the crystallite size of c-PeNC films and remove the remaining long-chain ligands (Figure 10b,c).[157] The chemical bonding is stronger between [PbI$_6$]$^{4-}$ and pyridine than between long-chain ligands and c-PeNCs, so the pyridine can separate the long-chain ligand from the surface of c-PeNCs. Subsequently, IPA efficiently removes the remaining long-chain ligands. In addition, pyridine and [PbI$_6$]$^{4-}$ would form a complex that interacts with FAI, and promotes the RP. Notably, the mild RP and the high concentration of FAI that is used in this method provide robust passivation for c-PeNC films. The method yielded a high average PCE = 16.46%, and a high J_{sc} = 19.30 mA cm^{-2}.

In summary, proper post-treatment can effectively increase PCEs of NC-PeSCs.

3.5. Device-Structure Engineering

Engineering of device architectures can yield high-efficiency NC-PeSCs. A suboptimal design in device structure can impede charge transport between the c-PeNC film and the ETL or HTL.

Heterojunction structures can facilitate charge dissociation and extraction. When polycrystalline PVK film is used, sequentially spin coating of two different types of PVK layers is difficult because the process uses polar solvents. A PVK layer that is applied on an underlying layer can damage it. In contrast, c-PeNCs are dispersed in non-polar solvents, so a c-PeNC heterojunction can be easily fabricated using two distinct types of c-PeNCs. When only one type c-PeNC layer is used, the space-charge region is wide; it is the primary cause of poor charge transfer and trap-assisted recombination (**Figure 11**a). Conversely, that had narrow space-charge region in heterojunction structure

**ADVANCED
SCIENCE NEWS**

www.advancedsciencenews.com
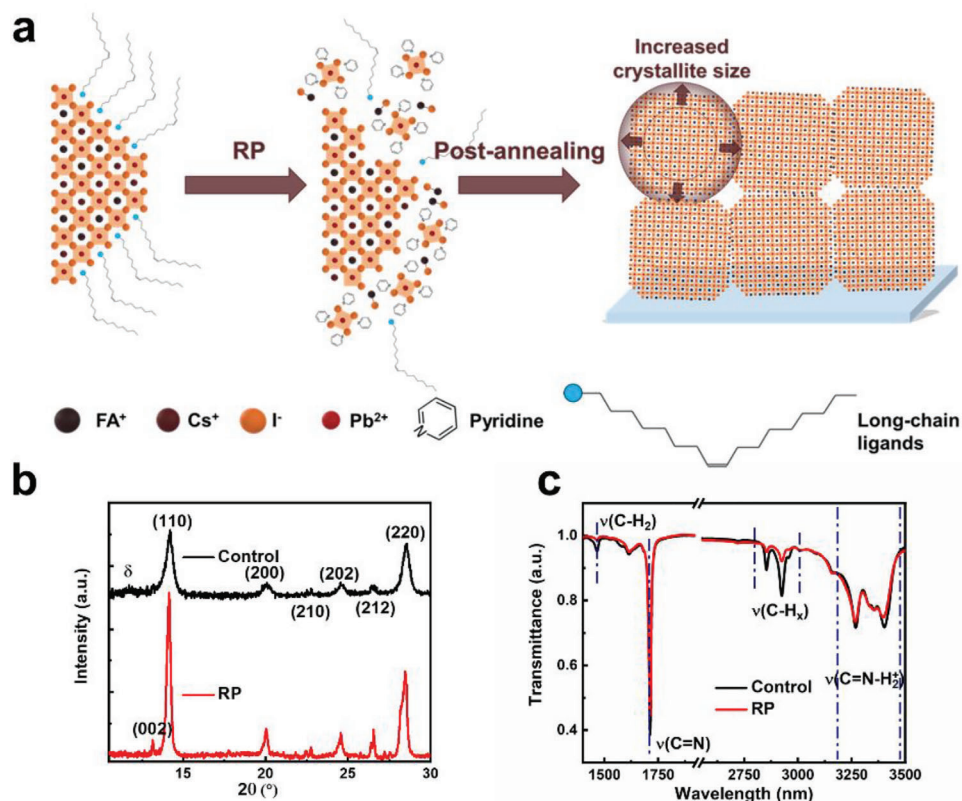
**ADVANCED
MATERIALS**

www.advmat.de

Figure 10. a) The schematic of the re-assembling process (RP) for c-PeNC films. b) The XRD pattern and c) FTIR spectra of control and RP samples. Reproduced with permission.[157] Copyright 2023, Wiley-VCH.

c-PeNC films, beneficial for exciton dissociations and charge transport.

A $CsPbI_3$/$FAPbI_3$ c-PeNC heterojunction structure has been obtained using a spin-coating method to deposit $FAPbI_3$ NCs on a $CsPbI_3$ NC layer.[159] This bilayer of $CsPbI_3$ and $FAPbI_3$ formed a graded energy-band structure, leading to facilitated charge separation; the resulting device was stable under humid conditions, and had PCE = 15.6%. Similarly, mixed-cation c-PeNCs that incorporate Cs^+ and FA^+ formed a heterostructure with $CsPbI_3$ NCs, and also improved the charge separation.[160]

Figure 11. a) Schematic of normal structure and heterojunction structure c-PeNC films. b) Energy-level alignment of c-PeNC films with diverse transporting layers.

However, the process complexity is increased when it uses a heterojunction that is formed by using c-PeNCs that have different compositions. To solve this problem, 2,2′-(perfluoronaphthalene-2,6-diylidene) dimalononitrile (F6TCNQ) can be doped into the array of $CsPbI_3$ NCs to augment charge transfer.[105] $CsPbI_3$ NCs have n-type semiconductor properties, whereas F6TCNQ-doped $CsPbI_3$ NCs have p-type properties. The combination of n-type and p-type nanocrystal layers yields in a homo-junction structure thereby increasing the stability of NC-PeSCs and their PCE to 15.29%.[105] Because of the increased charge extraction, the PCE of NC-PeSCs can still exceed 12% even if the c-PeNC layer is >1 μm thick.[105]

Device structure can also be modified by interface engineering. A ligand-exchange process introduces surface defects, which may result in poor energy alignment between the PVK layer and the charge transport layer. Passivating the interface of c-PeNCs facilitates charge separation and extraction. A 3D star-shaped organic semiconductor, known as Star-TrCN, has been used to passivate the surface of $CsPbI_3$ NCs.[161] It was directly spin-coated onto the $CsPbI_3$ NC layer, and then the -CN functional group in the Star-TrCN molecule interacted with Cs atoms on the surface of $CsPbI_3$ NCs. As a result, Star-TrCN passivated these surfaces, and yielded well-matched energy alignment with transporting layers; as a result, the PCEs were increased to 16.0%. The Star-TrCN also prevented moisture from infiltrating the c-PeNCs layer, so the operational stability of NC-PeSCs under ambient conditions was improved. Similarly, non-fullerene conjugate (Y6) molecules
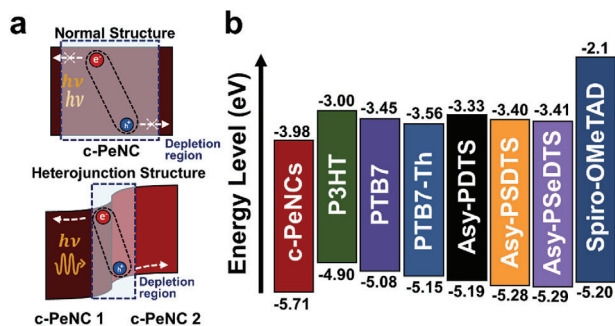
ADVANCED
SCIENCE NEWS
www.advancedsciencenews.com
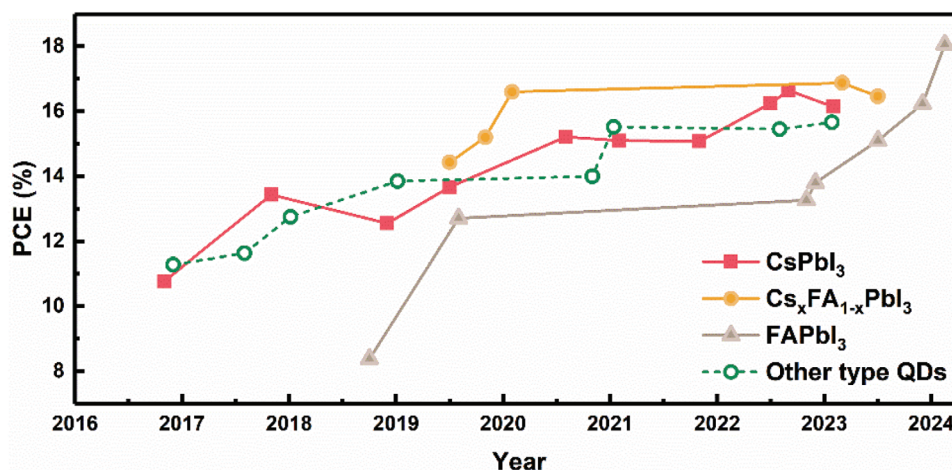
ADVANCED
MATERIALS
www.advmat.de

Figure 12. Evolution of PCE of NC-PeSCs of various compositions, and SCs based on other type QDs. The PCEs of SCs based on other type QDs—refer to refs. [165–172].

can be applied to passivate the surface of c-PeNCs.[162] These results demonstrated effective passivation of functional conjugated molecular on the interface between c-PeNC films and transporting layers, and yielded favorable energy alignment.

Selecting appropriate transporting layers to build good energy alignment and block minority carriers, is also crucial for effective carrier collection (Figure 11b). Poly[4,8-bis[(2-ethylhexyl)oxy]benzo[1,2-b:4,5-b′]dithiophene-2,6-diyl-alt-3-fluoro-2-[(2-ethylhexyl)carbonyl]thieno[3,4-b]thiophene-4,6-diyl] (PTB7) has been used as a dopant-free organic HTL.[163] Spiro-OMeTAD typically requires doping with various materials (e.g., Li-FTSI, tert-butylpyridine) to augment its hole mobility, but this method degrades device stability. Consequently, to extend the operational lifetime of NC-PeSCs, a dopant-free HTL must be applied. The use of PTB7 reduced hysteresis and improved stability. PTB7 could also form an effective passivation layer for CsPbI$_3$ NCs, and its favorable energy alignment enables efficient charge extraction. Therefore, the use of PTB7 achieved superior device PCE compared to the use of Spiro-OMeTAD.

A donor-acceptor conjugated polymeric material named Asy-PSeDTS has delocalized aromaticity caused by polar Se atoms. This characteristic increases the intermolecular interactions in Asy-PSeDTS, so it can increase charge transfer between Asy-PSeDTS HTL and c-PeNC films.[164] CsPbI$_3$ NC-PeSCs with Asy-PSeDTS had higher PCE and better stability compared to those that used the conventional Spiro-OMeTAD.

In summary, optimal structure engineering can facilitate exciton dissociation and carrier extraction, and thereby boost the PCE of NC-PeSCs.

High-efficiency NC-PeSCs have been achieved using various compositions of c-PeNCs (**Table 1**), and the PCE of NC-PeSCs is higher than that of SCs based on other type quantum dots (**Figure 12**). The use of the methods mentioned earlier has achieved NC-PeSCs with champion PCE > 18%, which is a remarkable 60% increase over the past 7 years. Notably, most reported NC-PeSCs use CsPbI$_3$ NCs as the absorbers; relatively few use FAPbI$_3$ NCs and they have inferior PCEs. Most of the NC-PeSCs that achieved the highest PCEs use mixed-cation c-PeNCs,

but the increase in PCE is only ≈1% compared to NC-PeSCs that use CsPbI$_3$ NCs.

Despite the advances, the PCEs and operational lifetimes must be increased considerably before commercialization is viable. Such advances require an increased understanding of the fundamental aspects of NC-PeSCs.

4. Unsolved Challenges

Despite the rapid increases that have been achieved in the PCEs of NC-PeSCs, they still have lower PCEs than PC-PeSCs. Several challenges currently hinder further advances in the PCEs of NC-PeSCs (**Figure 13**).

4.1. Low Short-Circuit Current Density

The primary obstacle to the increase in the PCE of NC-PeSCs is their low J_{sc}. The highest achieved J_{sc} of NC-PeSC stands at ≈20.93 mA cm^{-2}, whereas PC-PeSCs can easily reach 25 mA cm^{-2}.[154,182] NC-PeSCs have low V_{oc} loss, but the large difference in J_{sc} between NC-PeSCs and PC-PeSCs makes the PCE of NC-PeSC lower than that of PC-PeSCs.

During the generation of photocurrent, the absorber must first absorb photons that have energy equal to or larger than its bandgap, to excite carriers from the ground state to excited state, generating excitons. The build-in potential in SCs dissociates these excitons into free carriers, which travel along the absorber to the corresponding electrodes. As free carriers reach the interface of the absorber and transporting layer, they are extracted by transporting layer and conducted to external circuits, where they output photocurrent. This process reveals several factors that influence J_{sc}. These are discussed in the next passages.

4.1.1. Photon Absorption and Exciton Density

The number of photons that can be absorbed by the absorber determines the number of excitons that are generated. At a given

Table 1. Device performance parameters of NC-PeSCs that use c-PeNCs of various compositions.

Composition	Scan direction	V_{oc} [V]	J_{sc} [mA cm^{-2}]	FF [%]	PCE [%]	Refs.
CsPbI$_3$	Reverse	1.23	13.47	65	10.77	[37]
CsPbI$_3$	Reverse	1.1626	15.246	76.63	13.43	[173]
FAPbI$_3$	Forward	1.10	11.83	64.42	8.38	[174]
CsPbI$_3$	–	1.27	12.39	80	12.55	[163]
CsPbI$_2$Br	Reverse	1.3	5.32	77	5.34	[175]
	Forward	1.21	4.75	48	2.78	
Cs$_{0.25}$FA$_{0.75}$PbI$_3$/CsPbI$_3$	Reverse	1.20	18.91	76	17.39	[160]
	Forward	1.15	18.61	54	11.46	
	Average	1.18 ± 0.03	18.76 ± 0.15	65 ± 11	14.43 ± 2.97	
FAPbI$_3$	Negligible hysteresis	1.10	15.4	74.8	12.7	[134]
CsPbI$_3$/FAPbI$_3$ bilayer	Reverse	1.22	17.26	74	15.6	[159]
	Forward	1.20	17.21	72	14.9	
	Average	1.20 ± 0.02	16.70 ± 0.56	74 ± 2	15.2 ± 0.4	
CsPbI$_3$	Reverse	1.251	15.85	76.7	15.21	[176]
	Average	1.245	15.61	74.9	14.55	
Cs$_{0.5}$FA$_{0.5}$PbI$_3$	Reverse	1.17	18.3	78.3	16.6	[123]
CsPbI$_3$	–	1.25	14.32	79	14.25	[132]
CsPbI$_3$	Reverse	1.248	14.96	75.6	14.10	[149]
	Forward	1.248	14.89	75.3	14.00	
	Average	1.240 ± 0.010	14.66 ± 0.56	75 ± 2	13.67 ± 0.21	
CsPbI$_3$	–	1.26	15.2	78	15.1	[146]
CsPbI$_3$	–	1.27	17.71	72	16.21	[177]
CsPbI$_3$	Reverse	1.23	15.54	79.45	15.21	[138]
	Forward	1.22	15.42	79.34	14.93	
	Average	1.23 ± 0.01	15.48 ± 0.06	79.40 ± 0.06	15.07 ± 0.14	
CsPbI$_3$	Reverse	1.251	17.12	71.4	15.29	[105]
	Forward	1.251	16.9	71	15.01	
	Average	1.251 ± 0.00	17.01 ± 0.11	71.2 ± 0.2	15.15 ± 0.14	
CsPbI$_3$	Reverse	1.264	16.34	74.2	15.33	[138]
	Average	1.234 ± 0.08	15.72 ± 0.19	73.7 ± 12.6	14.97 ± 0.17	
CsPbI$_3$	Reverse	1.20	15.65	75.1	14.14	[145]
CsPbI$_3$	Non-negligible hysteresis	1.27	17.80	73.1	16.53	[158]
CsPbI$_3$	Non-negligible hysteresis	1.23	17.73	74.5	16.25	[117]
CsPbI$_3$	Non-negligible hysteresis	1.26	17.65	74.8	16.64	[178]
FAPbI$_3$	Reverse	0.89	14.56	78.6	10.13	[179]
	Average	0.88 ± 0.02	14.33 ± 0.32	76.7 ± 1.0	9.62 ± 0.29	
FAPbI$_3$	Reverse	1.12	18.5	67	13.8	[180]
	Average	1.12 ± 0.014	18.63 ± 0.507	63 ± 1.8	13.26 ± 0.327	
FAPbI$_3$	Reverse	1.15	18.45	68.2	14.47	[147]
	Forward	1.152	18.15	68.5	14.39	
	Average	1.141 ± 0.011	17.98 ± 0.15	66.3 ± 1.9	13.80 ± 0.48	
CsPbI$_3$	–	1.262	16.83	76	16.14	[181]
FA$_{0.36}$Cs$_{0.64}$PbI$_3$	Champion	1.23	18.99	74.0	17.29	[124]
	Average	1.228 ± 0.010	18.848 ± 0.184	73.0 ± 1.2	16.874 ± 0.237	

(Continued)

Table 1. (Continued)

Composition	Scan direction	V_{oc} [V]	J_{sc} [mA cm^{-2}]	FF [%]	PCE [%]	Refs.
FAPbI$_3$	Reverse	1.145	17.39	75	15.10	[124]
	Forward	1.155	17.27	72	14.41	
FAPbI$_3$	Champion	1.17	19.30	71.82	16.23	[148]
	Average	1.12 ± 0.004	19.25 ± 0.0033	70.24 ± 0.539	15.80 ± 0.145	
FAPbI$_3$	Reverse	1.16	20.80	79	18.93	[154]
	Forward	1.14	20.48	77	18.28	
	Certified	1.14 ± 0.01	20.89 ± 0.44	76 ± 1	18.06 ± 0.47	
Cs$_x$FA$_{1-x}$PbI$_3$	Reverse	1.15	19.31	75.13	16.68	[157]
	Forward	1.17	19.36	71.65	16.23	
	Average	1.16 ± 0.01	19.34 ± 0.03	73.39 ± 1.74	16.46 ± 0.23	

bandgap and composition, the thickness of the absorber significantly affects the number of photons that it can absorb. c-PeNCs film in NC-PeSCs are about 0.3 μm thick, whereas polycrystalline PVK films in PC-PeSCs are ≈0.5–1 μm thick.[20,183] Consequently, the exciton density is lower in c-PeNC film than in polycrystalline PVK films. Therefore, to increase J_{sc}, the thickness of c-PeNC films must be increased. However, increased thickness alone might not elevate J_{sc} if the following factors are not considered.

4.1.2. Exciton Binding Energy (E_b)

E_b affects the number of excitons that can be converted to free carriers. In PC-PeSCs, E_b is lower than the room temperature energy, so the exciton can easily dissociate to become a free car-rier. In contrast, the E_b of c-PeNC films is larger than the room temperature energy, so exciton dissociation is difficult in c-PeNC films.[184] Because of their high E_b, they may radiatively combine rather than separate, thereby reducing the number of excitons that can be converted to free carriers.[185] The high E_b of c-PeNC film is due to the nano-size induced charge confinement.[185] Thus, solving this problem entails reducing E_b by increasing the crystallite size of c-PeNC film.

Two methods may solve this problem. One is to increase the crystallite size of c-PeNC films, like the RP method;[157] the other is to increase the photo-recycling efficiency.[186] Fortunately, a high E_b is beneficial to increase the radiative recombination ratio of carriers. Although neither radiative nor non-radiative recombination processes are desirable in SCs, high radiative
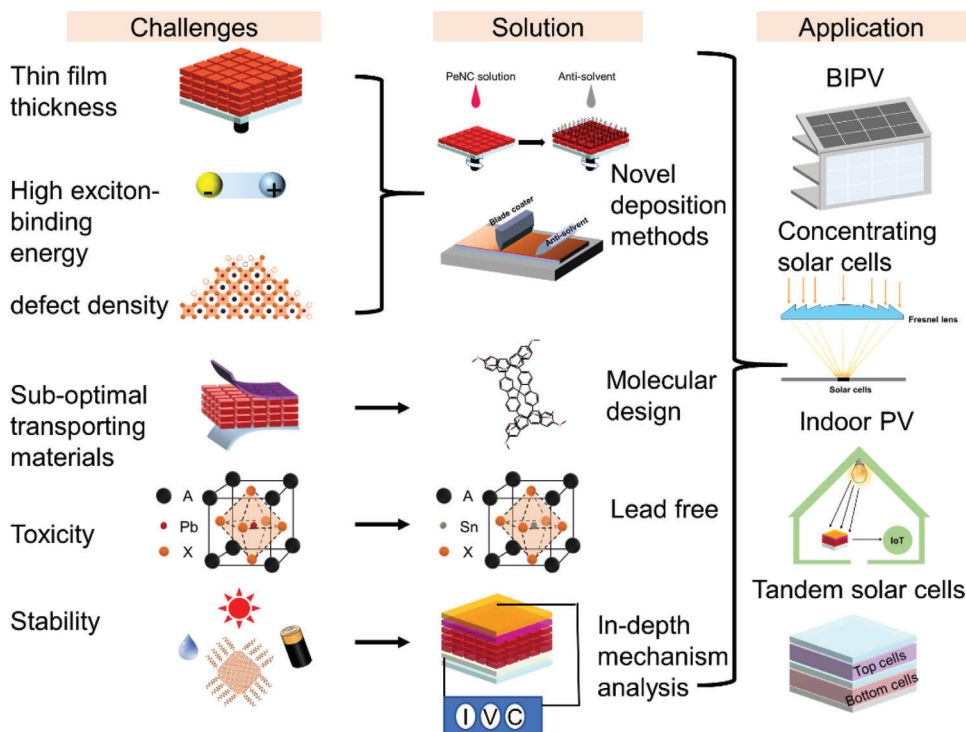

Figure 13. Challenges, solutions, and future applications for NC-PeSCs.

ADVANCED
SCIENCE NEWS

www.advancedsciencenews.com

ADVANCED
MATERIALS

www.advmat.de

recombination ratios can increase the photo-recycling efficiency, and thereby increase the efficiency at which excitons are converted to free carriers. Photo-recycling has been reported to increase the PCE of PC-PeSCs, but little similar work has been done for NC-PeSCs.[187,188]

Organic photovoltaics (OPV) also have high E_b, but it has little effect on their J_{sc}.[189,190] This result has been attributed to the charge-transfer state in the interface of the donor-acceptor in the OPV.[190] Therefore, building a similar charge-transfer structure in NC-PeSCs may also be a promising way to facilitate exciton dissociation. In short, the high E_b and its influence on J_{sc} need more attention, but ways to reduce E_b have not been sufficiently investigated.

4.1.3. Defect Density

The defect density significantly affects the carrier-transport and carrier-collection processes, which determine the EQE of NC-PeSCs.[191] Many strategies have been used to remove the long-chain ligands and passivate the defects, but the defect density increases exponentially as the thickness of active layers increases.[192] These defects trap free carriers and induce non-radiative recombination, which reduces J_{sc}.

Also, the EQE of NC-PeSCs is much lower at long wavelengths than at short wavelengths. This result occurs because photo carriers have less energy and must be transported farther to extraction layers when generated by long-wavelength photons than by short-wavelength photons. These effects increase their susceptibility to trap-assisted non-radiative recombination loss during transport, and cause decrease in EQE at long wavelengths. Solving this problem requires development of a method to increase the effectiveness of methods to passivate defects in NC-PeSC that use thick c-PeNC films.

In summary, increasing the J_{sc} is the most critical challenge to further increase the PCE of NC-PeSCs. Overcoming this challenge necessitates concurrent increase in c-PeNC film thickness, facilitated exciton dissociation, and reduced defect density.

4.2. Suboptimal Charge-Transporting Layer

The charge transporting layers in NC-PeSCs are typically adapted from those used in PC-PeSCs, such as SnO_2 or TiO_2 as ETL, and Spiro-OMeTAD or PTAA as HTL. Nevertheless, the surface properties of polycrystalline PVK films and c-PeNC films are fundamentally different. Therefore, to further increase the PCE of NC-PeSCs, the charge-transport layers must be optimized and customized.

Spiro-OMeTAD is the most widely-used HTL for NC-PeSCs, but it has inherently low hole mobility, so additives must be used, like 4-tert-butylpyridine (4-tBP) or bis(trifluoromethane)sulfonimide lithium salt (Li-TFSI).[193] However, additives may compromise the stability of Spiro-OMeTAD.[194] To address this problem, polymers like PTAA can be used as HTLs in PVK SCs, as an alternative to Spiro-OMeTAD.[195] For example, PTAA has been used as the HTL in $CsPbI_3$/$FAPbI_3$ NC-PeSCs.[196] However, a significant energy mismatch in the highest occupied molecular orbital (HOMO)

between the NCs and PTAA resulted in diminished PCE of NC-PeSCs. To address this energy disparity, an interfacial layer could be introduced between the NCs and the HTL, but this strategy increases the complexity of the device structure. As a result, optimal HTLs are not available for regular-structure NC-PeSCs.

Currently, the inverted p-i-n structure is prevalent in PC-PeSCs for its operational stability and integrity, particularly in tandem devices.[197] However, few efforts have been made to implement the p-i-n structure NC-PeSCs. A graphene electrode instead of silver has been placed on top of the NCs layer to achieve semitransparent NC-PeSCs that have the structure ITO/PTAA/$CsPbI_3$ NCs/C60/BCP/Graphene, but they had a low PCE = 6.8%.[198] PTAA has been evaluated as the HTL in NC-PeSCs that had either n-i-p or p-i-n structures, utilizing PTAA as the HTL.[199] Typically, c-PeNCs are dispersed in a non-polar solvent like octane or chlorobenzene. In p-i-n structure, PTAA is partially solvated when c-PeNC solution is spin-coated onto PTAA film. Compared to PTAA, PEDOT:PSS and NiO_x do not have this problem because they are less sensitive than PTAA to the solvent. Inverted $FAPbI_3$ NC-PeSCs with the structure ITO/PEDOT:PSS/$FAPbI_3$ NCs/PCBM/BCP/Ag had PCE = 10.13%.[179] Also, inverted $CsPbI_3$ NC-PeSCs with the structure FTO/NiO_x/$CsPbI_3$ NCs/C60/ZnO/Ag, fabricated by implementing FAI treatment layer-by-layer, achieved PCE = 13.1%.[153]

Despite these advances, inverted NC-PeSCs have lower PCEs and are less stable than regular n-i-p NC-PeSCs. This difference is attributed to the HTL which significantly affects the quality of c-PeNC films in p-i-n structure. Bonding between PEDOT:PSS and NC-PeSCs is relatively weak, so c-PeNC films easily shrink as long-chain ligands are removed during the ligand-exchange process. Consequently, c-PeNC films can delaminate from the substrates. In addition, the conductivity of PEDOT:PSS and NiO_x are not very good, so they have inferior carrier transport. Thus, another challenge is to develop an optimal HTL for inverted NC-PeSCs.

In conclusion, considering the different surface properties of c-PeNCs with polycrystalline PVK films, development of novel transporting materials that can strongly bond with c-PeNCs and have good conductivity is a challenge. Enriching the diversity of transporting materials will facilitate further improvement of NC-PeSCs.

4.3. Toxicity

Currently, most of the highly-efficient and stable NC-PeSCs use a PVK that has lead ions (Pb^{2+}) as the B-site cation. However, PVKs easily degrade, and thus form PbI_2, which is a highly toxic compound and can bio-accumulate in the ecosystem,[200] so several countries have banned products that contain more than a certain amount of lead. Therefore, commercialization of NC-PeSCs will require lead-free PVKs.

The most feasible candidate for lead-free PVK SCs uses Sn^{2+} as the B-site cation (e.g., $MASnI_3$, $FASnI_3$.). However, Sn^{2+} is easily oxidized to Sn^{4+}, and this process generates defects in the PVK structure.[142] $CsSnX_3$ (X = Cl, Br, and I) quantum rods synthesized using a typical hot-injection method have been applied to SCs. The SC that used $CsSnI_3$ quantum rods

**ADVANCED
SCIENCE NEWS**

www.advancedsciencenews.com

**ADVANCED
MATERIALS**

www.advmat.de

showed PCE = 12.96% with E_b = 2.0 eV.[201] Besides, SCs that use $CH_3NH_3SnBr_{3-x}I_x$ NCs presented PCE = 8.79%.[202] Germanium ion (Ge^{2+}) is another candidate for use as the B-site cation in lead-free PVK. Ge is non-toxic, but Ge^{2+} is also easily oxidized to Ge^{4+}.[203] B-site co-alloying of Ge and Sn to synthesize $CsSn_{0.6}Ge_{0.4}I_3$ NCs yielded NC-PeSCs that had very low PCE, due to a non-idea bandgap and a large number of defect states. The development of optimal synthesis methods to mitigate defect density in lead-free PVK c-PeNCs remains a challenge.

Double-PVK structures ($A_2B^+B^{3+}X_6$) also present alternatives for lead-free PVK. Elements such as bismuth (Bi) and antimony (Sb) can form double-PVK compounds like $Cs_2Ag(Bi/Sb)Br_6$.[204] SCs that used $Cs_2AgBi_{0.6}Sb_{0.4}Br_6$ NCs for SCs achieved PCE = 0.09%,[205] SCs that used $Cs_2AgBiBr_6$-NC had PCE = 0.46%.[206] However, these double-PVKs have an indirect bandgap, which limits their application in SCs.

In summary, the quest for lead-free NC-PeSCs that have high PCE remains a challenge. The development of sustainable and efficient photovoltaic technology requires the discovery of new suitable PVK structure materials that do not include lead.

4.4. Instability

The instability of optoelectronic devices that use PVKs remains a substantial hurdle to their commercial viability. Compared to polycrystalline PVKs, c-PeNCs have better phase stability, but the NC-PeSCs durability is still limited by the following several factors.

Surface properties strongly affect the stability of c-PeNCs.[84] Long-chained ligands dynamically attach to the surface of c-PeNC by ionic interaction or hydrogen bonding; these processes stabilize the amine and halides on the surface. The long-chained ligands are hydrophobic; this property and steric hindrance can prevent oxygen and water from penetrating the core of c-PeNCs. However, c-PeNC films are assembled lay-by-layer with MeOAc rinsing at every cycle, then post-treated using a polar solvent with FAI. As a result, large numbers of ligands are washed away, so under-coordinated sites develop on the surface of c-PeNCs, and ion distribution becomes disordered. Moreover, under long-term operation, proton-type surface defects induce formation of labile ammonium-amine species by the interaction of carboxylic acid and amine in ligands.[207] The under-coordinated sites provide reaction sites for water and oxygen, and serve as catalyzer, inducing poor durability of NC-PeSCs.[208] In addition, continuous light illumination activates surface defects that generate a local electrical field, which increases electron-phonon coupling and distorts the lattice, degrading the PCE of NC-PeSCs.[209]

Heat, humidity, illumination, and external electrical fields challenge the stability of NC-PeSCs. Environmental stresses also cause instability in NC-PeSCs. Some c-PeNCs, especially in $CsPbI_3$ c-PeNC film which has a low tolerance factor, are sensitive to heat, so they can transform into an undesired phase during thermal annealing.[210] FA is hygroscopic, and this property accelerates degradation in a high-humidity environment. Moreover, illumination and electrical fields induce ion migrations, which degrade the PCEs of NC-PeSCs.[211] Some reports have demonstrated suppressed ion migration in low-dimensional PVK materials, owing to steric hindrance by long-chained ligands, but the absence of ion migration in c-PeNC films remains to be demonstrated experimentally.[212]

The mechanisms that degrade NC-PeSCs warrant further investigation. Existing studies often borrow insights from PC-PeSCs or focus solely on c-PeNC degradation.[20] However, the surface properties, interface properties, chemical composition, and deposition process of c-PeNC films in NC-PeSCs are unique to PC-PeSCs.

To increase the stability of NC-PeSCs, their defects must be passivated, and the degradation mechanisms must be understood and overcome.

5. Conclusion and Outlook

This review has summarized recent advances that have increased the PCE of NC-PeSCs, and the challenges that remain before they can be commercialized. The PCE of NC-PeSCs has been increased beyond those of other quantum-dot SCs by methods such as in situ doping, ligand engineering, surface passivation, post-treatment, and device structure engineering. However, both the PCE and the stability of NC-PeSCs are still inferior to those of PC-PeSCs.

The low J_{sc} is the major limitation on the PCE of NC-PeSCs. Effective methods to increase J_{sc} are required. Furthermore, the sub-optimal transporting materials in NC-PeSCs do not permit efficient carrier extraction. The toxicity and chemical instability of NC-PeSCs also limits their applications. To further facilitate the development of NC-PeSCs, we suggest some solutions to address the major challenges for NC-PeSCs, and identify some potential applications of future NC-PeSCs (Figure 13).

5.1. Solutions

5.1.1. Novel Deposition Process

To sufficiently absorb sunlight, the c-PeNC film thickness should be increased, while retaining high carrier mobility and low defect density. Current fabrication techniques for c-PeNC films involve a layer-by-layer approach with repeated MeOAc rinsing and a final EtOAc post-treatment, but these methods cannot easily produce thick films that have excellent charge-transport properties. With too much rinse time and post-treating time, the c-PeNC films easily delaminate and degrade as loss of ligands. This process also inevitably introduces surface defects. Moreover, although many liquid- and solid-state ligand-exchange methods have been developed to improve the ligand-exchange efficiency, most of them are complex, yet still do not remove all of the long-chain ligands.

Alternative deposition methods must be developed to increase the thickness of c-PeNC films, increase carrier mobility, and decrease the number of defects. One-step spin-coating with anti-solvent dripping during spin-coating is widely used to fabricate polycrystalline PVK films, and can obtain thick and uniform polycrystalline PVK films. However, fabrication of a thick c-PeNC film by one-step spin coating is rarely reported. To fully exploit the advantages of c-PeNCs, other solution processing methods, such spray-coating, ink-jet printing, nozzle printing, and blade-coating

should be evaluated. These methods have been used to fabricate other solution-processed optoelectronic devices; we believe that learning more about these methods, especially those used in PC-PeSCs, would provide insights into how to develop novel deposition methods for NC-PeSCs.

5.1.2. Designing Novel Transporting Layers

The most-frequently reported NC-PeSC is deposited on SnO_2 or TiO_2 substrate. Few papers have reported NC-PeSC deposited on PTAA, PEDOT, NiO_x, or other transporting layers, and these NC-PeSCs had much lower PCEs than those deposited on SnO_2 or TiO_2. Also, c-PeNC films deposited on PTAA, PEDOT, or NiO_x are more susceptible to damage during rinsing by MeOAc than those deposited on SnO_2, but the reason for this susceptibility is not known. Properties of the substrate can significantly affect the crystal packing, orientation, and stability of c-PeNC films. The chemical properties and dipolar interaction between SnO_2 (or TiO_2)/c-PeNC differ from those between PEDOT (or PTAA, NiOx)/c-PeNC. Thus, in-depth understanding of these interface interactions must be obtained, to guide the development of novel substrate transporting layers, and to increase both the PCE and the stability of NC-PeSCs.

The top transporting layer is also important in NC-PeSCs. A good top layer should both passivate defects on the upper surface of the c-PeNC films and protect the c-PeNC film from damage by oxygen and moisture. The most-used top transporting layers in NC-PeSCs are spiro-OMeTAD and PCBM. Spiro-OMeTAD is expensive and requires careful doping to improve its conductivity, and this process can introduce unstable factors. PCBM film is too thin and unstable, so it cannot provide robust protection for NC-PeSCs. Future development of NC-PeSCs also requires the development of top transporting materials with high mobility and robust protection for underlying layer.

5.1.3. Machine Learning for Lead-Free PVK Materials

Machine learning (ML) analyzes extensive databases to offer guidance in designing and forecasting new materials. This approach can swiftly predict the characteristics of numerous novel materials while establishing correlations between specific attributes and desired outcomes. Moreover, its accuracy is comparable to that of the Density Functional Theory (DFT) method and finds fundamental physical principles conducive to guiding experimental synthesis. Consequently, the use of ML presents a viable method to achieve optimal lead-free PVK materials tailored for SC applications.

5.2. Applications

5.2.1. Semi-Transparent NC-PeSC for Building-Integrated Photovoltaic

The thinness of c-PeNC films limits its J_{sc} but presents an opportunity in building-integrated photovoltaic (BIPV) applications. The utilization of solar energy in cities is becoming increasingly

important. BIPV can convert solar energy to electrical power and reduce energy consumption in the building, and is therefore emerging as an important photovoltaic technology to fully utilize solar energy in cities. The excellent transparency of c-PeNC films makes them suitable as semi-transparent SCs for BIPV applications. The semi-transparent c-PeNCs could be used as glass curtain walls without influencing interior lighting, and they have a tunable bandgap that provides the possibility to make colorful glass, thereby improving the aesthetics of the building. Semi-transparent NC-PeSCs could also be used in self-powered electrochromic devices, like smart windows. Therefore, the use of semi-transparent NC-PeSCs as BIPVs is worthy of attention.

5.2.2. Concentrating SCs

Concentrating SCs are using optical devices to concentrate and redirect sunlight onto small-area SCs. When integrated with solar trackers and cooling systems, this setup yields substantial electrical energy from limited SC surface areas. Consequently, concentrating SCs provide a highly competitive photovoltaic technology. However, these cells operate under high temperatures and carrier densities, so the materials used must have appropriate stability. The exceptional thermal stability exhibited by c-PeNCs, particularly those that use $CsPbI_3$ NCs, positions them as potential candidates for application in concentrating SCs. Notably, c-PeNCs can slow down hot-carrier cooling under high excitation intensity. Consequently, concentrating SCs that use c-PeNCs offer the prospect of exploiting hot carriers, thereby potentially surpassing the Shockley-Queisser limitation and substantially increasing the PCEs. Further development of concentrating SCs requires investigation into the operational behavior of NC-PeSCs under high excitation intensity and elevated temperatures. To maximize the advantages offered by NC-PeSCs, this application warrants attention in future research.

5.2.3. Indoor Photovoltaic Devices

Indoor photovoltaic devices are designed to convert indoor light to electrical energy. Integration of indoor photovoltaic technology with electronic devices can reuse energy and substantially reduce energy consumption. However, the emission spectra of indoor light sources differ significantly from the standard AM1.5G spectrum, and have considerably lower intensity than sunlight. Consequently, the absorber that is used must have an appropriate bandgap. Theoretically, an optimal bandgap for indoor photovoltaic devices falls within the range of 1.8–1.95 eV. Remarkably, the bandgap of $CsPbI_3$ NCs is ≈1.8 eV, so they are highly promising candidates for indoor photovoltaic applications. Additionally, the low defect density in NC-PeSCs ensures exceptional PCE even under low illumination intensities. The use of NC-PeSCs as indoor photovoltaic devices holds substantial promise for future industry applications.

5.2.4. Tandem SCs

Constructing multi-junction SCs represents a feasible way to achieve high PCEs. To accomplish this, different bandgap SCs

should be carefully designed to ensure the full utilization of sun illuminations. The bandgap of c-PeNCs can be readily tuned by adjusting the size and composition of c-PeNCs, thus offering great potential in realizing different bandgap SCs. Moreover, attributed to the mild solution processing of PeNC films, NC-PeSCs can be easily integrated with various types of SCs, such as silicon SCs, organic photovoltaics, PC-PeSCs, and CIGS, enabling constructing tandem SCs. Pioneering efforts in incorporating PeNCs into tandem SCs have been reported. For example, CsPbI$_3$ NC-PeSCs with a bandgap of about 1.73 eV and low voltage loss, could serve as top SCs in all-PVK integrated tandem SCs.[213] Besides, the theoretical analysis has demonstrated that combining PC-PeSCs (1.55 eV) with narrow bandgap NC-PeSCs could yield high PCEs.[214] Thus, the NC-PeSCs is a promising candidate in tandem SCs, capable of functioning as both top and bottom SCs.

In conclusion, although there remain some challenges for the commercial application of NC-PeSCs, c-PeNCs still present great potential and advantage for photovoltaic applications in some special situation. We believe that NC-PeSCs will occupy an important position in the future photovoltaic market after more in-depth researches.

Conflict of Interest

The authors declare no conflict of interest.

[1] D. Luo, W. Yang, Z. Wang, A. Sadhanala, Q. Hu, R. Su, R. Shivanna, G. F. Trindade, J. F. Watts, Z. Xu, T. Liu, K. Chen, F. Ye, P. Wu, L. Zhao, J. Wu, Y. Tu, Y. Zhang, X. Yang, W. Zhang, R. H. Friend, Q. Gong, H. J. Snaith, R. Zhu, *Science* **2018**, *360*, 1442.

[2] J. S. Kim, J.-M. Heo, G.-S. Park, S.-J. Woo, C. Cho, H. J. Yun, D.-H. Kim, J. Park, S.-C. Lee, S.-H. Park, E. Yoon, N. C. Greenham, T.-W. Lee, *Nature* **2022**, *611*, 688.

[3] Y.-H. Chiang, K. Frohna, H. Salway, A. Abfalterer, L. Pan, B. Roose, M. Anaya, S. D. Stranks, *ACS Energy Lett.* **2023**, *8*, 2728.

[4] W. Yang, R. Su, D. Luo, Q. Hu, F. Zhang, Z. Xu, Z. Wang, J. Tang, Z. Lv, X. Yang, Y. Tu, W. Zhang, H. Zhong, Q. Gong, T. P. Russell, R. Zhu, *Nano Energy* **2020**, *67*, 104189.

[5] https://www.nrel.gov/pv/assets/pdfs/best-research-cell-efficiencies.pdf, **2024.04.04**.

[6] X. Yang, D. Luo, Y. Xiang, L. Zhao, M. Anaya, Y. Shen, J. Wu, W. Yang, Y. H. Chiang, Y. Tu, R. Su, Q. Hu, H. Yu, G. Shao, W. Huang, T. P. Russell, Q. Gong, S. D. Stranks, W. Zhang, R. Zhu, *Adv. Mater.* **2021**, *33*, 2006435.

[7] Y. Zheng, S. Yang, *Sol. RRL* **2022**, *6*, 2100710.

[8] Q. Hu, W. Chen, W. Yang, Y. Li, Y. Zhou, B. W. Larson, J. C. Johnson, Y.-H. Lu, W. Zhong, J. Xu, L. Klivansky, C. Wang, M. Salmeron, A. B. Djurisic, F. Liu, Z. B. He, R. Zhu, T. P. Russell, *Joule* **2020**, *4*, 1575.

[9] M. Kim, J. Jeong, H. Lu, T. K. Lee, F. T. Eickemeyer, Y. Liu, I. W. Choi, S. J. Choi, Y. Jo, H.-B. Kim, S.-I. Mo, K.-Y. Kim, H. Lee, N. G. An, S. Cho, W. R. Tress, S. M. Zakeeruddin, A. Hagfeldt, J. Y. Kim, M. Gratzel, D. S. Kim, *Science* **2022**, *375*, 302.

[10] P. Sun, G. Qu, Q. Hu, Y. Ma, H. Liu, Z.-X. Xu, Z. Huang, *ACS Appl. Energy Mater.* **2022**, *5*, 3568.

[11] Y.-H. Kim, C. Wolf, Y.-T. Kim, H. Cho, W. Kwon, S. Do, A. Sadhanala, C. G. Park, S.-W. Rhee, S. H. Im, R. H. Friend, T.-W. Lee, *ACS Nano* **2017**, *11*, 6586.

[12] D. Han, M. Imran, M. Zhang, S. Chang, X.-g. Wu, X. Zhang, J. Tang, M. Wang, S. Ali, X. Li, G. Yu, J. Han, L. Wang, B. Zou, H. Zhong, *ACS Nano* **2018**, *12*, 8808.

[13] Y. Wu, X. Li, H. Zeng, *ACS Energy Lett.* **2019**, *4*, 673.

[14] S. Ju, C. Mao, J. Zheng, K. Yang, L. Lin, T. Guo, H. Hu, F. Li, *ACS Appl. Nano Mater.* **2023**, *6*, 9219.

[15] W. Chi, S. K. Banerjee, *Adv. Funct. Mater.* **2022**, *32*, 2200029.

[16] M. Xie, J. Guo, X. Zhang, C. Bi, L. Zhang, Z. Chu, W. Zheng, J. You, J. Tian, *Nano Lett.* **2022**, *22*, 8266.

[17] Y. Dong, Y.-K. Wang, F. Yuan, A. Johnston, Y. Liu, D. Ma, M.-J. Choi, B. Chen, M. Chekini, S.-W. Baek, L. K. Sagar, J. Fan, Y. Hou, M. Wu, S. Lee, B. Sun, S. Hoogland, R. Quintero-Bermudez, H. Ebe, P. Todorovic, F. Dinic, P. Li, H. T. Kung, M. I. Saidaminov, E. Kumacheva, E. Spiecker, L.-S. Liao, O. Voznyy, Z. H. Lu, E. H. Sargent, *Nat. Nanotechnol.* **2020**, *15*, 668.

[18] Y.-H. Kim, J. Park, S. Kim, J. S. Kim, H. Xu, S.-H. Jeong, B. Hu, T.-W. Lee, *Nat. Nanotechnol.* **2022**, *17*, 590.

[19] A. Liu, C. Bi, J. Li, M. Zhang, C. Cheng, D. Binks, J. Tian, *Nano Lett.* **2023**, *23*, 2405.

[20] S. Lim, S. Han, D. Kim, J. Min, J. Choi, T. Park, *Adv. Mater.* **2023**, *35*, 2203430.

[21] Y. Wang, Z. Lv, J. Chen, Z. Wang, Y. Zhou, L. Zhou, X. Chen, S. T. Han, *Adv. Mater.* **2018**, *30*, 1802883.

[22] I. Ryu, J. Y. Ryu, G. Choe, H. Kwon, H. Park, Y. S. Cho, R. Du, S. Yim, *Adv. Funct. Mater.* **2021**, *31*, 2102334.

[23] T.-W. Lee, S. H. Im, Y.-H. Kim, H. Cho, US10193088B2, **2015**: KR101815588B1, 2015 (Priority date: 2014.11.06).

[24] T.-W. Lee, S. H. Im, H. Cho, Y.-H. Kim, US20220199933A1, **2022** (Priority date: 2014.11.06).

[25] Q. Wang, X. Zhang, Z. Jin, J. Zhang, Z. Gao, Y. Li, S. F. Liu, *ACS Energy Lett.* **2017**, *2*, 1479.

[26] Y. Lei, Y. Li, Z. Jin, *Energy Rev* **2022**, *1*, 100003.

[27] J. Zhang, J. Bai, Z. Jin, H. Bian, K. Wang, J. Sun, Q. Wang, S. Liu, *Adv. Energy Mater.* **2018**, *8*, 1703246.

[28] X. Zheng, J. Troughton, N. Gasparini, Y. Lin, M. Wei, Y. Hou, J. Liu, K. Song, Z. Chen, C. Yang, B. Turedi, A. Y. Alsalloum, J. Pan, J. Chen, A. A. Zhumekenov, T. D. Anthopoulos, Y. Han, D. Baran, O. F. Mohammed, E. H. Sargent, O. M. Bakr, *Joule* **2019**, *3*, 1963

[29] H. Bian, D. Bai, Z. Jin, K. Wang, L. Liang, H. Wang, J. Zhang, Q. Wang, S. Liu, *Joule* **2018**, *2*, 1500.

[30] H. Zhou, J. Park, Y. Lee, J.-M. Park, J.-H. Kim, J. S. Kim, H.-D. Lee, S. H. Jo, X. Cai, L. Li, X. Sheng, H. J. Yun, J.-W. Park, J.-Y. Sun, T.-W. Lee, *Adv. Mater.* **2020**, *32*, 2001989.

[31] L. C. Schmidt, A. Pertegás, S. González-Carrero, O. Malinkiewicz, S. Agouram, G. Minguez Espallargas, H. J. Bolink, R. E. Galian, J. Pérez-Prieto, *J. Am. Chem. Soc.* **2014**, *136*, 850.

[32] F. Zhang, H. Zhong, C. Chen, X.-g. Wu, X. Hu, H. Huang, J. Han, B. Zou, Y. Dong, *ACS Nano* **2015**, *9*, 4533.

[33] C. Ma, M. Zhang, J. Zhang, J. Liao, H. Sun, D. Ji, R. Pang, H. Zhang, J. Liu, S. Liu, *Adv. Funct. Mater.* **2024**, 2316717.

[34] Z. Bai, H. Zhong, *Sci. Bull.* **2015**, *60*, 1622.

[35] H. C. Wang, W. Wang, A. C. Tang, H. Y. Tsai, Z. Bao, T. Ihara, N. Yarita, H. Tahara, Y. Kanemitsu, S. Chen, R.-S. Liu, *Angew. Chem.* **2017**, *129*, 13838.

[36] C. B. Murray, D. J. Norris, M. G. Bawendi, *J. Am. Chem. Soc.* **1993**, *115*, 8706.

[37] A. Swarnkar, A. R. Marshall, E. M. Sanehira, B. D. Chernomordik, D. T. Moore, J. A. Christians, T. Chakrabarti, J. M. Luther, *Science* **2016**, *354*, 92.

[38] J. Chen, D. Jia, E. M. Johansson, A. Hagfeldt, X. Zhang, *Energy Environ. Sci.* **2021**, *14*, 224.

[39] J. A. Dias, S. H. Santagneli, S. J. Ribeiro, Y. Messaddeq, *Sol. RRL* **2021**, *5*, 2100205.

[40] M. V. Kovalenko, L. Protesescu, M. I. Bodnarchuk, *Science* **2017**, *358*, 745.

[41] H. C. Woo, J. W. Choi, J. Shin, S.-H. Chin, M. H. Ann, C.-L. Lee, *J. Phys. Chem. Lett.* **2018**, *9*, 4066.

[42] S.-H. Jo, W. Yang, Y. Tang, D.-H. Kim, W. Lee, J. Park, S. E. Chang, S. Y. Lim, S. Kim, Y. S. Lee, J. Y. Kim, J. Kim, B. Hu, K. Zhu, T.-W. Lee, *ACS Energy Lett.*, https://doi.org/10.1021/acsenergylett.4c00928.

[43] D. N. Minh, J. Kim, J. Hyon, J. H. Sim, H. H. Sowlih, C. Seo, J. Nam, S. Eom, S. Suk, S. Lee, E. Kim, Y. Kang, *Chem. Mater.* **2017**, *29*, 5713.

[44] L. Peng, A. Tang, C. Yang, F. Teng, *J. Alloys Compd.* **2016**, *687*, 506.

[45] C. Zhang, J. Chen, S. Wang, L. Kong, S. W. Lewis, X. Yang, A. L. Rogach, G. Jia, *Adv. Mater.* **2020**, *32*, 2002736.

[46] X. Liu, R. Hong, C. Tian, *J. Mater. Sci.: Mater. Electron.* **2009**, *20*, 323.

[47] C. Sun, Y. Zhang, C. Ruan, C. Yin, X. Wang, Y. Wang, W. W. Yu, *Adv. Mater.* **2016**, *28*, 10088.

[48] M. Saliba, T. Matsui, K. Domanski, J.-Y. Seo, A. Ummadisingu, S. M. Zakeeruddin, J.-P. Correa-Baena, W. R. Tress, A. Abate, A. Hagfeldt, M. Grätzel, *Science* **2016**, *354*, 206.

[49] J.-P. Correa-Baena, A. Abate, M. Saliba, W. Tress, T. Jesper Jacobsson, M. Grätzel, A. Hagfeldt, *Energy Environ. Sci.* **2017**, *10*, 710.

[50] D. B. Straus, S. Guo, A. M. Abeykoon, R. J. Cava, *Adv. Mater.* **2020**, *32*, 2001069.

[51] C. Wang, A. S. R. Chesman, J. J. Jasieniak, *Chem. Commun.* **2017**, *53*, 232.

[52] F. Ke, C. Wang, C. Jia, N. R. Wolf, J. Yan, S. Niu, T. P. Devereaux, H. I. Karunadasa, W. L. Mao, Y. Lin, *Nat. Commun.* **2021**, *12*, 461.

[53] C. Bi, S. V. Kershaw, A. L. Rogach, J. Tian, *Adv. Funct. Mater.* **2019**, *29*, 1902446.

[54] T. A. Berhe, W.-N. Su, C.-H. Chen, C.-J. Pan, J.-H. Cheng, H.-M. Chen, M.-C. Tsai, L.-Y. Chen, A. A. Dubale, B.-J. Hwang, *Energy Environ. Sci.* **2016**, *9*, 323.

[55] J. Bisquert, E. J. Juarez-Perez, *J. Phys. Chem. Lett.* **2019**, *10*, 5889.

[56] G. S. Selopal, H. Zhao, Z. M. Wang, F. Rosei, *Adv. Funct. Mater.* **2020**, *30*, 1908762.

[57] H. Zhu, N. Song, T. Lian, *J. Am. Chem. Soc.* **2010**, *132*, 15038.

[58] B. Mahler, B. Nadal, C. Bouet, G. Patriarche, B. Dubertret, *J. Am. Chem. Soc.* **2012**, *134*, 18591.

[59] P. Reiss, M. Protiere, L. Li, *Small* **2009**, *5*, 154.

[60] G. H. Ahmed, J. Yin, O. M. Bakr, O. F. Mohammed, *ACS Energy Lett.* **2021**, *6*, 1340.

[61] W. Chen, S. Bhaumik, S. A. Veldhuis, G. Xing, Q. Xu, M. Grätzel, S. Mhaisalkar, N. Mathews, T. C. Sum, *Nat. Commun.* **2017**, *8*, 15198.

[62] N. J. Simi, S. B. Bernadsha, A. Thomas, V. V. Ison, *Results Opt.* **2021**, *4*, 100088.

[63] C. Zhang, S. Wang, X. Li, M. Yuan, L. Turyanska, X. Yang, *Adv. Funct. Mater.* **2020**, *30*, 1910582.

[64] C. Tan, J. Chen, X.-J. Wu, H. Zhang, *Nat. Rev. Mater.* **2018**, *3*, 17089.

[65] A. M. Smith, S. Nie, *Acc. Chem. Res.* **2010**, *43*, 190.

[66] C. Jia, H. Li, X. Meng, H. Li, *Chem. Commun.* **2018**, *54*, 6300.

[67] X. Tang, J. Yang, S. Li, Z. Liu, Z. Hu, J. Hao, J. Du, Y. Leng, H. Qin, X. Lin, Y. Lin, Y. Tian, M. Zhou, Q. Xiong, *Adv. Sci.* **2019**, *6*, 1900412.

[68] X. Liu, X. Zhang, L. Li, J. Xu, S. Yu, X. Gong, J. Zhang, H. Yin, *ACS Appl. Mater. Interfaces* **2019**, *11*, 40923.

[69] Y. Huang, F. Li, L. Qiu, F. Lin, Z. Lai, S. Wang, L. Lin, Y. Zhu, Y. Wang, Y. Jiang, X. Chen, *ACS Appl. Mater. Interfaces* **2019**, *11*, 26384.

[70] Z. Li, L. Kong, S. Huang, L. Li, *Angew. Chem.* **2017**, *129*, 8246.

[71] J. Cassidy, M. Zamkov, *J. Chem. Phys.* **2020**, *152*, 110902.

[72] Z. Xie, X. Li, R. Li, S. Lu, W. Zheng, D. Tu, Y. Feng, X. Chen, *Nanoscale* **2020**, *12*, 17113.

[73] A. Buin, P. Pietsch, J. Xu, O. Voznyy, A. H. Ip, R. Comin, E. H. Sargent, *Nano Lett.* **2014**, *14*, 6281.

[74] S. D. Stranks, G. E. Eperon, G. Grancini, C. Menelaou, M. J. P. Alcocer, T. Leijtens, L. M. Herz, A. Petrozza, H. J. Snaith, *Science* **2013**, *342*, 341.

[75] S. W. Dai, B. W. Hsu, C. Y. Chen, C. A. Lee, H. Y. Liu, H. F. Wang, Y. C. Huang, T. L. Wu, A. Manikandan, R. M. Ho, C.-S. Tsao, C.-H. Cheng, Y.-L. Chueh, H.-W. Lin, *Adv. Mater.* **2018**, *30*, 1705532.

[76] Y.-H. Kim, S. Kim, A. Kakekhani, J. Park, J. Park, Y.-H. Lee, H. Xu, S. Nagane, R. B. Wexler, D.-H. Kim, S. H. Jo, L. Martinez-Sarti, P. Tan, A. Sadhanala, G.-S. Park, Y.-W. Kim, B. Hu, H. J. Bolink, S. Yoo, R. H. Friend, R. A. M. T.-W. Lee, *Nat. Photonics* **2021**, *15*, 148.

[77] Y. Chen, S. R. Smock, A. H. Flintgruber, F. A. Perras, R. L. Brutchey, A. J. Rossini, *J. Am. Chem. Soc.* **2020**, *142*, 6117.

[78] S. ten Brinck, I. Infante, *ACS Energy Lett.* **2016**, *1*, 1266.

[79] J. Pan, L. N. Quan, Y. Zhao, W. Peng, B. Murali, S. P. Sarmah, M. Yuan, L. Sinatra, N. M. Alyami, J. Liu, E. Yassitepe, Z. Yang, O. Voznyy, R. Comin, M. N. Hedhili, O. F. Mohammed, Z. H. Lu, D. H. Kim, E. H. Sargent, B. O. M, *Adv. Mater.* **2016**, *28*, 8718.

[80] J. C. Hamill Jr., J. Schwartz, Y.-L. Loo, *ACS Energy Lett.* **2017**, *3*, 92.

[81] K. Hoshi, T. Chiba, J. Sato, Y. Hayashi, H. Takahashi, H. Ebe, S. Ohisa, J. Kido, *ACS Appl. Mater. Interfaces* **2018**, *10*, 24607.

[82] P. Liu, W. Chen, W. Wang, B. Xu, D. Wu, J. Hao, W. Cao, F. Fang, Y. Li, Y. Zeng, R. Pan, S. Chen, W. Cao, X. W. Sun, K. Wang, *Chem. Mater.* **2017**, *29*, 5168.

[83] B. A. Koscher, J. K. Swabeck, N. D. Bronstein, A. P. Alivisatos, *J. Am. Chem. Soc.* **2017**, *139*, 6566.

[84] Y. Bai, M. Hao, S. Ding, P. Chen, L. Wang, *Adv. Mater.* **2022**, *34*, 2105958.

[85] R. Wang, Y. Shang, P. Kanjanaboos, W. Zhou, Z. Ning, E. H. Sargent, *Energy Environ. Sci.* **2016**, *9*, 1130.

[86] Q. Xiong, S. Huang, J. Du, X. Tang, F. Zeng, Z. Liu, Z. Zhang, T. Shi, J. Yang, D. Wu, H. Lin, Z. Luo, Y. Leng, *Adv. Opt. Mater.* **2020**, *8*, 2000977.

[87] J. Owen, *Science* **2015**, *347*, 615.

[88] Y. K. Wang, K. Singh, J. Y. Li, Y. Dong, X. Q. Wang, J. M. Pina, Y. J. Yu, R. Sabatini, Y. Liu, D. Ma, J. Liu, Z. Liu, Y. Gao, O. Voznyy, W. Ma, M.-K. Fung, L.-S. Liao, E. H. Sargent, *Adv. Mater.* **2022**, *34*, 2200854.

[89] F. Liu, J. Jiang, Y. Zhang, C. Ding, T. Toyoda, S. Hayase, R. Wang, S. Tao, Q. Shen, *Angew. Chem.* **2020**, *132*, 8499.

[90] T. Chiba, Y. Hayashi, H. Ebe, K. Hoshi, J. Sato, S. Sato, Y.-J. Pu, S. Ohisa, J. Kido, *Nat. Photonics* **2018**, *12*, 681.

[91] S. Park, H. Cho, W. Choi, H. Zou, D. Y. Jeon, *Nanoscale Adv.* **2019**, *1*, 2828.

[92] C. Bi, Z. Yao, X. Sun, X. Wei, J. Wang, J. Tian, *Adv. Mater.* **2021**, *33*, 2006722.

[93] A. Pan, B. He, X. Fan, Z. Liu, J. J. Urban, A. P. Alivisatos, L. He, Y. Liu, *ACS Nano* **2016**, *10*, 7943.

[94] J. De Roo, N. Yazdani, E. Drijvers, A. Lauria, J. Maes, J. S. Owen, I. Van Driessche, M. Niederberger, V. Wood, J. C. Martins, *Chem. Mater.* **2018**, *30*, 5485.

[95] L. M. Wheeler, E. M. Sanehira, A. R. Marshall, P. Schulz, M. Suri, N. C. Anderson, J. A. Christians, D. Nordlund, D. Sokaras, T. Kroll, S.

P. Harvey, J. J. Berry, L. Y. Lin, J. M. Luther, *J. Am. Chem. Soc.* **2018**, *140*, 10504.

[96] D. P. Nenon, J. A. Christians, L. M. Wheeler, J. L. Blackburn, E. M. Sanehira, B. Dou, M. L. Olsen, K. Zhu, J. J. Berry, J. M. Luther, *Energy Environ. Sci.* **2016**, *9*, 2072.

[97] S. Seth, A. Samanta, *Sci. Rep.* **2016**, *6*, 37693.

[98] Z. Liu, Y. Bekenstein, X. Ye, S. C. Nguyen, J. Swabeck, D. Zhang, S.-T. Lee, P. Yang, W. Ma, A. P. Alivisatos, *J. Am. Chem. Soc.* **2017**, *139*, 5309.

[99] H. Li, Q. Wang, Y. Oteki, C. Ding, D. Liu, Y. Guo, Y. Li, Y. Wei, D. Wang, Y. Yang, T. Masuda, M. Chen, Z. Zhang, T. Sogabe, S. Hayase, Y. Okada, S. Iikubo, Q. Shen, *Adv. Mater.* **2023**, *35*, 2301834.

[100] B. Yu, L. Chen, Z. Qu, C. Zhang, Z. Qin, X. Wang, M. Xiao, *J. Phys. Chem. Lett.* **2021**, *12*, 238.

[101] M. Li, S. Bhaumik, T. W. Goh, M. S. Kumar, N. Yantara, M. Grätzel, S. Mhaisalkar, N. Mathews, T. C. Sum, *Nat. Commun.* **2017**, *8*, 14350.

[102] C. Ding, F. Liu, Y. Zhang, D. Hirotani, X. Rin, S. Hayase, T. Minemoto, T. Masuda, R. Wang, Q. Shen, *Nano Energy* **2020**, *67*, 104267.

[103] S. Kahmann, M. A. Loi, *J. Mater. Chem. C* **2019**, *7*, 2471.

[104] G. Conibeer, N. Ekins-Daukes, J.-F. Guillemoles, D. Kőnig, E.-C. Cho, C.-W. Jiang, S. Shrestha, M. Green, *Sol. Energy Mater. Sol. Cells* **2009**, *93*, 713.

[105] X. Zhang, H. Huang, X. Ling, J. Sun, X. Jiang, Y. Wang, D. Xue, L. Huang, L. Chi, J. Yuan, W. Ma, *Adv. Mater.* **2022**, *34*, 2105977.

[106] J. Yang, X. Wen, H. Xia, R. Sheng, Q. Ma, J. Kim, P. Tapping, T. Harada, T. W. Kee, F. Huang, Y.-B. Cheng, M. Green, A. Ho-Baillie, S. Huang, S. Shrestha, R. Patterson, G. Conibeer, *Nat. Commun.* **2017**, *8*, 14120.

[107] J. Fu, Q. Xu, G. Han, B. Wu, C. H. A. Huan, M. L. Leek, T. C. Sum, *Nat. Commun.* **2017**, *8*, 1300.

[108] Z. Nie, Z. Huang, M. Zhang, B. Wu, H. Wu, Y. Shi, K. Wu, Y. Wang, *ACS Photonics* **2022**, *9*, 3457.

[109] V. Kumar, V. Nagal, S. Srivastava, M. Kumar, B. K. Gupta, A. K. Hafiz, K. Singh, *ChemistrySelect* **2021**, *6*, 10165.

[110] X. Liu, P. Zeng, S. Chen, T. A. Smith, M. Liu, *Laser Photonics Rev.* **2022**, *16*, 2200280.

[111] L. Dai, Z. Deng, F. Auras, H. Goodwin, Z. Zhang, J. C. Walmsley, P. D. Bristowe, F. Deschler, N. C. Greenham, *Nat. Photonics* **2021**, *15*, 696.

[112] M. E. Madjet, G. R. Berdiyorov, F. El-Mellouhi, F. H. Alharbi, A. V. Akimov, S. Kais, *J. Phys. Chem. Lett.* **2017**, *8*, 4439.

[113] H. Benisty, C. Sotomayor-Torres, C. Weisbuch, *Phys. Rev. B* **1991**, *44*, 10945.

[114] A. Forde, T. Inerbaev, E. K. Hobbie, D. S. Kilin, *J. Am. Chem. Soc.* **2019**, *141*, 4388.

[115] G. Kaur, K. J. Babu, H. N. Ghosh, *J. Phys. Chem. Lett.* **2020**, *11*, 6206.

[116] V. Klimov, M. Mikhailovsky, D. McBranch, C. Leatherdale, M. Bawendi, *Science* **2000**, *287*, 1011.

[117] J. Chen, D. Jia, R. Zhuang, Y. Hua, X. Zhang, *Adv. Mater.* **2022**, *34*, 2204259.

[118] C. Bi, X. Sun, X. Huang, S. Wang, J. Yuan, J. X. Wang, T. Pullerits, J. Tian, *Chem. Mater.* **2020**, *32*, 6105.

[119] S. Bera, D. Ghosh, A. Dutta, S. Bhattacharyya, S. Chakraborty, N. Pradhan, *ACS Energy Lett.* **2019**, *4*, 1364.

[120] J. Kim, S. Cho, F. Dinic, J. Choi, C. Choi, S. M. Jeong, J.-S. Lee, O. Voznyy, M. J. Ko, Y. Kim, *Nano Energy* **2020**, *75*, 104985.

[121] Y. Li, F. Z. Liu, M. Waqas, T. L. Leung, H. W. Tam, X. Q. Lan, B. Tu, W. Chen, A. B. Djurišić, Z. B. He, *Small Methods* **2018**, *2*, 1700387.

[122] X. Shen, B. M. Gallant, P. Holzhey, J. A. Smith, K. A. Elmestekawy, Z. Yuan, P. V. G. M. Rathnayake, S. Bernardi, A. Dasgupta, E. Kasparavicius, T. Malinauskas, P. Caprioglio, O. Shargaieva, Y.-H. Lin, M. M. McCarthy, E. Unger, V. Getautis, A. Widmer-Cooper, L. M. Herz, H. J. Snaith, *Adv. Mater.* **2023**, *35*, 2211742.

[123] M. Hao, Y. Bai, S. Zeiske, L. Ren, J. Liu, Y. Yuan, N. Zarrabi, N. Cheng, M. Ghasemi, P. Chen, M. Lyu, D. He, J.-H. Yun, Y. Du, Y. Wang, S. Ding, A. Armin, P. Meredith, G. Liu, H.-M. Cheng, L. Wang, *Nat. Energy* **2020**, *5*, 79.

[124] D. Jia, J. Chen, R. Zhuang, Y. Hua, X. Zhang, *Adv. Mater.* **2023**, *35*, 2212160.

[125] J. Zhang, Y. Zhong, L. Chen, L. Yang, *Chem. Phys. Lett.* **2020**, *752*, 137572.

[126] L. Zhang, C. Kang, G. Zhang, Z. Pan, Z. Huang, S. Xu, H. Rao, H. Liu, S. Wu, X. Wu, X. Li, Z. Zhu, X. Zhong, A. K.-Y. Jen, *Adv. Funct. Mater.* **2021**, *31*, 2005930.

[127] J. Shi, F. Li, J. Yuan, X. Ling, S. Zhou, Y. Qian, W. Ma, *J. Mater. Chem. A* **2019**, *7*, 20936.

[128] Q. Wang, Z. Jin, D. Chen, D. Bai, H. Bian, J. Sun, G. Zhu, G. Wang, S. Liu, *Adv. Energy Mater.* **2018**, *8*, 1800007.

[129] S. R. Smock, T. J. Williams, R. L. Brutchey, *Angew. Chem., Int. Ed.* **2018**, *57*, 11711.

[130] T. Zhu, D. Zheng, M.-N. Rager, T. Pauporté, *Sol. RRL* **2020**, *4*, 2000348.

[131] D. Jia, J. Chen, M. Yu, J. Liu, E. M. J. Johansson, A. Hagfeldt, X. Zhang, *Small* **2020**, *16*, 2001772.

[132] J. Khan, X. Zhang, J. Yuan, Y. Wang, G. Shi, R. Patterson, J. Shi, X. Ling, L. Hu, T. Wu, S. Dai, W. Ma, *ACS Energy Lett.* **2020**, *5*, 3322.

[133] Y. Wang, J. Yuan, X. Zhang, X. Ling, B. W. Larson, Q. Zhao, Y. Yang, Y. Shi, J. M. Luther, W. Ma, *Adv. Mater.* **2020**, *32*, 2000449.

[134] J. Xue, R. Wang, L. Chen, S. Nuryyeva, T.-H. Han, T. Huang, S. Tan, J. Zhu, M. Wang, Z.-K. Wang, C. Zhang, J.-W. Lee, Y. Yang, *Adv. Mater.* **2019**, *31*, 1900111.

[135] Y. Wang, C. Duan, X. Zhang, J. Sun, X. Ling, J. Shi, L. Hu, Z. Zhou, X. Wu, W. Han, X. Liu, C. Cazorla, D. Chu, S. Huang, T. Wu, J. Yuan, W. Ma, *Adv. Funct. Mater.* **2022**, *32*, 2108615.

[136] K. Chen, Q. Zhong, W. Chen, B. Sang, Y. Wang, T. Yang, Y. Liu, Y. Zhang, H. Zhang, *Adv. Funct. Mater.* **2019**, *29*, 1900991.

[137] F. Li, X. Zhang, J. Shi, L. Jin, J. Qiao, J. Guo, H. Yin, Y. Li, J. Yuan, W. Ma, *Adv. Funct. Mater.* **2023**, *33*, 2302542.

[138] Y. Shi, L. Yuan, Z. Liu, Y. Lu, B. Yuan, W. Shen, B. Xue, Y. Zhang, Y. Qian, F. Li, X. Zhang, Y. Liu, Y. Wang, L. Wang, J. Yuan, L.-S. Liao, B. Yang, Y. Yu, W. Ma, *ACS Nano* **2022**, *16*, 10534.

[139] J. Jiang, F. Liu, Q. Shen, S. Tao, *J. Mater. Chem. A* **2021**, *9*, 12087.

[140] S. Wang, Q. Zhao, A. Hazarika, S. Li, Y. Wu, Y. Zhai, X. Chen, J. M. Luther, G. Li, *Nat. Commun.* **2023**, *14*, 2216.

[141] E. T. Vickers, T. A. Graham, A. H. Chowdhury, B. Bahrami, B. W. Dreskin, S. Lindley, S. B. Naghadeh, Q. Qiao, J. Z. Zhang, *ACS Energy Lett.* **2018**, *3*, 2931.

[142] Y. Su, J. Yang, G. Liu, W. Sheng, J. Zhang, Y. Zhong, L. Tan, Y. Chen, *Adv. Funct. Mater.* **2022**, *32*, 2109631.

[143] X. Zhang, H. Huang, Y. M. Maung, J. Yuan, W. Ma, *Chem. Commun.* **2021**, *57*, 7906.

[144] J. Shi, F. Li, Y. Jin, C. Liu, B. Cohen-Kleinstein, S. Yuan, Y. Li, Z. K. Wang, J. Yuan, W. Ma, *Angew. Chem.* **2020**, *132*, 22414.

[145] R. Han, Q. Zhao, A. Hazarika, J. Li, H. Cai, J. Ni, J. Zhang, *ACS Appl. Mater. Interfaces* **2022**, *14*, 4061.

[146] L. Hu, Q. Zhao, S. Huang, J. Zheng, X. Guan, R. Patterson, J. Kim, L. Shi, C.-H. Lin, Q. Lei, D. Chu, W. Tao, S. Cheong, R. D. Tilley, A. W. Y. Ho-Baillie, J. M. Luther, J. Yuan, T. Wu, *Nat. Commun.* **2021**, *12*, 466.

[147] X. Zhang, H. Huang, L. Jin, C. Wen, Q. Zhao, C. Zhao, J. Guo, C. Cheng, H. Wang, L. Zhang, Y. Li, Y. Maung Maung, J. Yuan, W. Ma, *Angew. Chem., Int. Ed.* **2023**, *62*, 202214241.

[148] M. Li, Y. Bao, W. Hui, K. Sun, L. Gu, X. Kang, D. Wang, B. Wang, H. Deng, R. Guo, Z. Li, X. Jiang, P. Muller-Buschbaum, L. Song, W. Huang, *Adv. Mater.* **2024**, *36*, 2309890.

**ADVANCED
SCIENCE NEWS**

www.advancedsciencenews.com

**ADVANCED
MATERIALS**

www.advmat.de

[149] X. Ling, S. Zhou, J. Yuan, J. Shi, Y. Qian, B. W. Larson, Q. Zhao, C. Qin, F. Li, G. Shi, C. Stewart, J. Hu, X. Zhang, J. M. Luther, S. Duhm, W. Ma, *Adv. Energy Mater.* **2019**, *9*, 1900721.

[150] J. Chen, D. Jia, J. Qiu, R. Zhuang, Y. Hua, X. Zhang, *Nano Energy* **2022**, *96*, 107140.

[151] K. Chen, W. Jin, Y. Zhang, T. Yang, P. Reiss, Q. Zhong, U. Bach, Q. Li, Y. Wang, H. Zhang, Q. Bao, Y. Liu, *J. Am. Chem. Soc.* **2020**, *142*, 3775.

[152] J. Kim, B. Koo, W. H. Kim, J. Choi, C. Choi, S. J. Lim, J.-S. Lee, D.-H. Kim, M. J. Ko, Y. Kim, *Nano Energy* **2019**, *66*, 104130.

[153] S. B. Shivarudraiah, M. Ng, C. H. A. Li, J. E. Halpert, *ACS Appl. Energy Mater.* **2020**, *3*, 5620.

[154] H. Aqoma, S.-H. Lee, I. F. Imran, J.-H. Hwang, S.-H. Lee, S.-Y. Jang, *Nat. Energy* **2024**, *9*, 324.

[155] Q. Jiang, Y. Zhao, X. Zhang, X. Yang, Y. Chen, Z. Chu, Q. Ye, X. Li, Z. Yin, J. You, *Nat. Photonics* **2019**, *13*, 460.

[156] R. Yu, G. Wu, R. Shi, Z. Ma, Q. Dang, Y. Qing, C. Zhang, K. Xu, Z. A. Tan, *Adv. Energy Mater.* **2023**, *13*, 2203127.

[157] W. Yang, S.-H. Jo, Y. Tang, J. Park, S. G. Ji, S. H. Cho, Y. Hong, D.-H. Kim, J. Park, E. Yoon, H. Zhou, S.-J. Woo, H. Kim, H. J. Yun, Y. S. Lee, J. Y. Kim, B. Hu, T.-W. Lee, *Adv. Mater.* **2023**, *35*, 2304533.

[158] D. Jia, J. Chen, J. Qiu, H. Ma, M. Yu, J. Liu, X. Zhang, *Joule* **2022**, *6*, 1632.

[159] F. Li, S. Zhou, J. Yuan, C. Qin, Y. Yang, J. Shi, X. Ling, Y. Li, W. Ma, *ACS Energy Lett.* **2019**, *4*, 2571.

[160] Q. Zhao, A. Hazarika, X. Chen, S. P. Harvey, B. W. Larson, G. R. Teeter, J. Liu, T. Song, C. Xiao, L. Shaw, M. Zhang, G. Li, M. C. Beard, J. M. Luther, *Nat. Commun.* **2019**, *10*, 2842.

[161] S. Lim, D. H. Lee, H. Choi, Y. Choi, D. G. Lee, S. B. Cho, S. Ko, J. Choi, Y. Kim, T. Park, *Nano Micro Lett.* **2022**, *14*, 204.

[162] J. Yuan, X. Zhang, J. Sun, R. Patterson, H. Yao, D. Xue, Y. Wang, K. Ji, L. Hu, S. Huang, D. Chu, T. Wu, J. Hou, J. Yuan, *Adv. Funct. Mater.* **2021**, *31*, 2101272.

[163] J. Yuan, X. Ling, D. Yang, F. Li, S. Zhou, J. Shi, Y. Qian, J. Hu, Y. Sun, Y. Yang, X. Gao, S. Duhm, Q. Zhang, W. Ma, *Joule* **2018**, *2*, 2450.

[164] D. H. Lee, S. Lim, C. Kim, H. U. Lee, D. Chung, Y. Choi, J. Choi, Y. Kim, S. B. Cho, H. I. Kim, T. Park, *ACS Energy Lett.* **2023**, *8*, 1839.

[165] M. Liu, O. Voznyy, R. Sabatini, F. P. García de Arquer, R. Munir, A. H. Balawi, X. Lan, F. Fan, G. Walters, A. R. Kirmani, S. Hoogland, F. Laquai, A. Amassian, E. H. Sargent, *Nat. Mater.* **2017**, *16*, 258.

[166] J. Choi, Y. Kim, J. W. Jo, J. Kim, B. Sun, G. Walters, F. P. García de Arquer, R. Quintero-Bermudez, Y. Li, C. S. Tan, L. N. Quan, A. P. T. Kam, S. Hoogland, Z. Lu, O. Voznyy, E. H. Sargent, *Adv. Mater.* **2017**, *29*, 1702350.

[167] H. I. Kim, S.-W. Baek, H. J. Cheon, S. U. Ryu, S. Lee, M.-J. Choi, K. Choi, M. Biondi, S. Hoogland, F. P. G. de Arquer, S.-K. Kwon, Y.-H. Kim, T. Park, E. H. Sargent, *Adv. Mater.* **2020**, *32*, 2004985.

[168] C. Ding, D. Wang, D. Liu, H. Li, Y. Li, S. Hayase, T. Sogabe, T. Masuda, Y. Zhou, Y. Yao, Z. Zou, R. Wang, Q. Shen, *Adv. Energy Mater.* **2022**, *12*, 2201676.

[169] W. Wang, W. Feng, J. Du, W. Xue, L. Zhang, L. Zhao, Y. Li, X. Zhong, *Adv. Mater.* **2018**, *30*, 1705746.

[170] H. Zhang, W. Fang, W. Wang, N. Qian, X. Ji, *ACS Appl. Mater. Interfaces* **2019**, *11*, 6927.

[171] H. Song, Y. Lin, Z. Zhang, H. Rao, W. Wang, Y. Fang, Z. Pan, X. Zhong, *J. Am. Chem. Soc.* **2021**, *143*, 4790.

[172] H. Song, H. Mu, J. Yuan, B. Liu, G. Bai, S. Lin, *SusMat* **2023**, *3*, 543.

[173] E. M. Sanehira, A. R. Marshall, J. A. Christians, S. P. Harvey, P. N. Ciesielski, L. M. Wheeler, P. Schulz, L. Y. Lin, M. C. Beard, J. M. Luther, *Sci. Adv.* **2017**, *3*, eaao4204.

[174] J. Xue, J.-W. Lee, Z. Dai, R. Wang, S. Nuryyeva, M. E. Liao, S.-Y. Chang, L. Meng, D. Meng, P. Sun, O. Lin, M. S. Goorsky, Y. Yang, *Joule* **2018**, *2*, 1866.

[175] S. Christodoulou, F. Di Stasio, S. Pradhan, A. Stavrinadis, G. Konstantatos, *J. Phys. Chem. C* **2018**, *122*, 7621.

[176] X. Ling, J. Yuan, X. Zhang, Y. Qian, S. M. Zakeeruddin, B. W. Larson, Q. Zhao, J. Shi, J. Yang, K. Ji, Y. Zhang, Y. Wang, C. Zhang, S. Duhm, J. M. Luther, M. Grätzel, W. Ma, *Adv. Mater.* **2020**, *32*, 2001906.

[177] X. Cao, J. Li, H. Dong, P. Li, Q. Fan, R. Xu, H. Li, G. Zhou, Z. Wu, *Adv. Funct. Mater.* **2021**, *31*, 2104344.

[178] D. Jia, J. Chen, R. Zhuang, Y. Hua, X. Zhang, *Energy Environ. Sci.* **2022**, *15*, 4201.

[179] Y. Xu, H. Li, S. Ramakrishnan, D. Song, Y. Zhang, M. Cotlet, Q. Yu, *ACS Appl. Energy Mater.* **2022**, *5*, 9858.

[180] S. Ding, M. Hao, C. Fu, T. Lin, A. Baktash, P. Chen, D. He, C. Zhang, W. Chen, A. K. Whittaker, Y. Bai, L. Wang, *Adv. Sci.* **2022**, *9*, 2204476.

[181] H. Huang, X. Zhang, R. Gui, C. Zhao, J. Guo, Y. M. Maung, H. Yin, W. Ma, J. Yuan, *Adv. Funct. Mater.* **2023**, *33*, 2210728.

[182] S. M. Park, M. Wei, N. Lempesis, W. Yu, T. Hossain, L. Agosta, V. Carnevali, H. R. Atapattu, P. Serles, F. T. Eickemeyer, H. Shin, M. Vafaie, D. Choi, K. Darabi, E. D. Jung, Y. Yang, D. B. Kim, S. M. Zakeeruddin, B. Chen, A. Amassian, T. Filleter, M. G. Kanatzidis, K. R. Graham, L. Xiao, U. Rothlisberger, M. Grätzel, E. H. Sargent, *Nature* **2023**, *624*, 289.

[183] T. Kim, X. Jin, J. H. Song, S. Jeong, T. Park, *ACS Energy Lett.* **2019**, *5*, 248.

[184] X. Zhang, L. Guo, Y. Zhang, C. Cheng, Y. Cheng, X. Li, J. Zhang, S. Xu, Y. Cao, B. Chen, *J. Non-Cryst. Solids* **2020**, *541*, 120066.

[185] Y. Jiang, X. Wang, A. Pan, *Adv. Mater.* **2019**, *31*, 1806671.

[186] L. M. Pazos-Outón, M. Szumilo, R. Lamboll, J. M. Richter, M. Crespo-Quesada, M. Abdi-Jalebi, H. J. Beeson, M. Vrućinić, M. Alsari, H. J. Snaith, *Science* **2016**, *351*, 1430.

[187] C. Cho, J.-W. Jang, S. Lee, Y. Vaynzof, M. Choi, J. H. Noh, K. Leo, *Sci. Adv.* **2021**, *7*, eabj1363.

[188] A. R. Bowman, M. Anaya, N. C. Greenham, S. D. Stranks, *Phys. Rev. Lett.* **2020**, *125*, 067401.

[189] H.-W. Li, Z. Guan, Y. Cheng, T. Lui, Q. Yang, C.-S. Lee, S. Chen, S.-W. Tsang, *Adv. Electron. Mater.* **2016**, *2*, 1600200.

[190] W. Xue, Y. Tang, X. Zhou, Z. Tang, H. Zhao, T. Li, L. Zhang, S. Liu, C. Zhao, W. Ma, H. Yan, *Adv. Funct. Mater.* **2021**, *31*, 2101892.

[191] G. Landi, H. C. Neitzert, C. Barone, C. Mauro, F. Lang, S. Albrecht, B. Rech, S. Pagano, *Adv. Sci.* **2017**, *4*, 1700183.

[192] S. T. Jan, M. Noman, *Sol. Energy* **2022**, *237*, 29.

[193] F. M. Rombach, S. A. Haque, T. J. Macdonald, *Energy Environ. Sci.* **2021**, *14*, 5161.

[194] Y. Shen, K. Deng, L. Li, *Small Methods* **2022**, *6*, 2200757.

[195] Y. Wang, L. Duan, M. Zhang, Z. Hameiri, X. Liu, Y. Bai, X. Hao, *Sol. RRL* **2022**, *6*, 2200234.

[196] K. Ji, J. Yuan, F. Li, Y. Shi, X. Ling, X. Zhang, Y. Zhang, H. Lu, J. Yuan, W. Ma, *J. Mater. Chem. A* **2020**, *8*, 8104.

[197] T. Liu, K. Chen, Q. Hu, R. Zhu, Q. Gong, *Adv. Energy Mater.* **2016**, *6*, 1600457.

[198] M. M. Tavakoli, M. Nasilowski, J. Zhao, M. G. Bawendi, J. Kong, *Small Methods* **2019**, *3*, 1900449.

[199] C. Xiao, Q. Zhao, C.-S. Jiang, Y. Sun, M. M. Al-Jassim, S. U. Nanayakkara, J. M. Luther, *Nano Energy* **2020**, *78*, 105319.

[200] W. Ke, M. G. Kanatzidis, *Nat. Commun.* **2019**, *10*, 965.

[201] L.-J. Chen, C.-R. Lee, Y.-J. Chuang, Z.-H. Wu, C. Chen, *J. Phys. Chem. Lett.* **2016**, *7*, 5028.

[202] H. Xu, H. Yuan, J. Duan, Y. Zhao, Z. Jiao, Q. Tang, *Electrochim. Acta* **2018**, *282*, 807.

[203] C. C. Stoumpos, L. Frazer, D. J. Clark, Y. S. Kim, S. H. Rhim, A. J. Freeman, J. B. Ketterson, J. I. Jang, M. G. Kanatzidis, *J. Am. Chem. Soc.* **2015**, *137*, 6804.

[204] P.-K. Kung, M.-H. Li, P.-Y. Lin, J.-Y. Jhang, M. Pantaler, D. C. Lupascu, G. Grancini, P. Chen, *Sol. RRL* **2020**, *4*, 1900306.

**ADVANCED
SCIENCE NEWS**

www.advancedsciencenews.com

**ADVANCED
MATERIALS**

www.advmat.de

[205] A. Kumar, S. K. Swami, S. Rawat, V. Singh, O. P. Sinha, R. Srivastava, *Int. J. Energy Res.* **2021**, *45*, 16769.

[206] R. Ahmad, G. V. Nutan, D. Singh, G. Gupta, U. Soni, S. Sapra, R. Srivastava, *Nano Res.* **2021**, *14*, 1126.

[207] E. Yassitepe, Z. Yang, O. Voznyy, Y. Kim, G. Walters, J. A. Castañeda, P. Kanjanaboos, M. Yuan, X. Gong, F. Fan, J. Pan, S. Hoogland, R. Comin, O. M. Bakr, L. A. Padilha, A. F. Nogueira, E. H. Sargent, *Adv. Funct. Mater.* **2016**, *26*, 8757.

[208] S.-C. Liu, Z. Li, Y. Yang, X. Wang, Y.-X. Chen, D.-J. Xue, J.-S. Hu, *J. Am. Chem. Soc.* **2019**, *141*, 18075.

[209] N. Ahn, K. Kwak, M. S. Jang, H. Yoon, B. Y. Lee, J.-K. Lee, P. V. Pikhitsa, J. Byun, M. Choi, *Nat. Commun.* **2016**, *7*, 13422.

[210] A. Dutta, S. K. Dutta, S. Das Adhikari, N. Pradhan, *Angew. Chem., Int. Ed.* **2018**, *57*, 9083.

[211] Z. Li, C. Xiao, Y. Yang, S. P. Harvey, D. H. Kim, J. A. Christians, M. Yang, P. Schulz, S. U. Nanayakkara, C.-S. Jiang, J. M. Luther, J. J. Berry, M. C. Beard, M. M. Al-Jassim, K. Zhu, *Energy Environ. Sci.* **2017**, *10*, 1234.

[212] Z. Huang, A. H. Proppe, H. Tan, M. I. Saidaminov, F. Tan, A. Mei, C.-S. Tan, M. Wei, Y. Hou, H. Han, S. O. Kelley, E. H. Sargent, *ACS Energy Lett.* **2019**, *4*, 1521.

[213] J. A. Christians, A. R. Marshall, Q. Zhao, P. Ndione, E. M. Sanehira, J. M. Luther, presented at 2018 IEEE 7th World Conf. on Photovoltaic Energy Conversion (WCPEC) (A Joint Conf. of 45th IEEE PVSC, 28th PVSEC & 34th EU PVSEC), IEEE, Piscataway, NJ **2018**, pp. 81–84.

[214] A. Karani, L. Yang, S. Bai, M. H. Futscher, H. J. Snaith, B. Ehrler, N. C. Greenham, D. Di, *ACS Energy Lett.* **2018**, *3*, 869.

Wenqiang Yang earned a B.S. in Physics from Huazhong University of Science and Technology in 2015 and received his Ph.D. in Optics from Peking University in 2020. Before he joined Beihang University, he worked as a post-doctoral researcher in Prof. Tae-Woo Lee's group at Seoul National University, in South Korea. He is now an associate professor at the International Research Institute for Multidisciplinary Science at Beihang University. His research focuses on optoelectronics based on organic–inorganic hybrid electronic materials for solar cells, light-emitting diodes, and photodetectors.

Seung-Hyeon Jo received his B.S. degree in the Department of Materials Science and Engineering at Seoul National University in 2017. He is currently a Ph.D. candidate student in the Department of Materials Science and Engineering at Seoul National University.

Tae-Woo Lee is a professor in MSE at Seoul National University, South Korea. He received his Ph.D. in Chemical Engineering from KAIST in 2002. He joined Bell Laboratories, USA, as a postdoctoral researcher and worked as a research staff at Samsung Advanced Institute of Technology (2003–2008). He was an associate professor at Pohang University of Science and Technology (POSTECH), South Korea, until 2016. He founded SN Display Co. Ltd. in 2020. His research focuses on soft printed electronics and optoelectronics based on organic and organic–inorganic hybrid electronic materials for flexible displays, solid-state lighting, solar energy conversion devices, and bioinspired neuromorphic devices.

2401788 (25 of 25)